coatings

MDPI

Review

Review of Progress in Marine Anti-Fouling Coatings: Manufacturing Techniques and Copper- and Silver-Doped Antifouling Coatings

Xiaolong Shi [1,2], Hua Liang [1,2] and Yanzhou Li [3,*]

[1] College of Automotive Engineering, Yancheng Institute of Technology, Yancheng 224051, China; shixiaolongycit@163.com (X.S.); lianghua@ycit.edu.cn (H.L.)
[2] College of Mechanical Engineering, Yancheng Institute of Technology, Yancheng 224051, China
[3] School of Mechanical and Vehicle Engineering, West Anhui University, Yueliangdao Road, No. 1, Lu'an 237010, China
* Correspondence: liyanzhou9336@163.com; Tel.: +86-15044211299

Abstract: Marine biofouling presents numerous challenges, including increased drag, reduced efficiency, and ecological imbalance. This review presents an overview of recent advances in antifouling coatings. First, essential preparation techniques such as cold spray, plasma spray, magnetron sputtering, and laser cladding are introduced, including the specific characteristics of each method. Next, the antifouling performance of Cu-doped and Ag-doped coating is analyzed. Emphasis is placed on the differences in coating composition, preparation methods, and their effects on antifouling and anticorrosion properties. The future development of antifouling technologies is also discussed, emphasizing the creation of multifunctional coatings, the optimization of coating microstructures for better performance, and the advancement of sustainable materials to minimize environmental impact.

Keywords: marine environment; antifouling coatings; Cu-doped antifouling coating; Ag-doped antifouling coating

Citation: Shi, X.; Liang, H.; Li, Y. Review of Progress in Marine Anti-Fouling Coatings: Manufacturing Techniques and Copper- and Silver-Doped Antifouling Coatings. *Coatings* **2024**, *14*, 1454. https://doi.org/10.3390/coatings14111454

Academic Editor: Jean-François Berret

Received: 13 October 2024
Revised: 8 November 2024
Accepted: 12 November 2024
Published: 15 November 2024

1. Introduction

Marine biofouling refers to the phenomenon where microorganisms, plants, and animals in the ocean attach to the surfaces of marine engineering equipment, ships, pipelines, and other artificial structures [1–11]. Over time, these organisms proliferate and grow on the surfaces, forming biofilms or biological communities. Marine biofouling causes various issues [9,12–17], including increased frictional resistance on ships and equipment, reduced operational efficiency, higher fuel consumption, and increased maintenance costs [9,18,19]. It can also affect the normal functioning of equipment, weaken structural durability, and raise the risk of malfunctions and accidents. Also, biofouling may spread invasive species, disrupting the balance of ecosystems and causing environmental problems [20]. As a result, marine biofouling has become a significant challenge in marine engineering and ecological protection.

To address marine biofouling, several methods have been developed, including physical removal [21,22], which involves manually or mechanically cleaning attached organisms; electrolysis of seawater [23–25], which kills organisms using highly oxidizing substances generated through electrolysis; and the direct addition of biocides, where chemicals are added to seawater to inhibit the growth of organisms. Additionally, antifouling coatings can be applied using specialized coatings to prevent biofouling [14,17,26]. Regarding the first three methods, physical removal is simple but inefficient and unable to eliminate microorganisms. Seawater electrolysis consumes a lot of energy and requires high initial investment costs, making it less viable for long-term applications. While adding biocides is effective, the chemicals are unstable, pose safety risks, affect environmental compatibility,

and are inconvenient for moving ships, making dynamic cleaning unfeasible. What sets the coating method apart from other approaches is its capacity to retain the substrate's original characteristics and simultaneously improve its surface performance with the coating. Adjusting the coating composition and processing techniques allows for targeted performance regulation, making it easier to maintain and repair. Therefore, current research focuses on the development and application of antifouling coatings.

In selecting coating protection methods, it is crucial to consider factors such as performance, service life, long-term adhesion, and cost while optimizing the choice based on specific application conditions. Marine antifouling coatings predominantly use organic materials, such as silicone-based and Cu-containing antifouling coatings [27–31]. However, in more demanding environments, such as deep-sea drilling platforms, submarine cables, and marine buoys, materials are required not only to have antifouling properties but also to possess adequate mechanical strength and wear resistance to maintain coating adhesion over time [32,33]. Therefore, the coating above applications presents certain limitations.

In contrast, metal-based and ceramic coatings [34–39], due to their higher hardness, better wear resistance, corrosion resistance, and longer service life, exhibit clear advantages. As a result, developing coatings with improved comprehensive surface properties, matched with appropriate preparation techniques, has become a key research focus in antifouling coatings. For example, the research includes the design of coating compositions with Cu as the primary antibacterial component [39–41], studies on the design and preparation processes of multilayer coating structures [42,43], performance studies of coatings with Ag as the main antibacterial component [44,45], and investigations into the mechanisms of performance enhancement for TiO_2 ceramic-phase composite-metal-based materials [31,35,46,47], etc. While much work has been done in this area, a systematic review remains lacking.

In summary, this review summarizes the main preparation techniques for high-surface-strength antifouling coatings, including cold spraying, plasma spraying, magnetron sputtering, and laser cladding. It then analyzes the key components, characteristics, and antifouling mechanisms of various coatings, such as Cu-doped polymers, Cu-doped metal coatings, Cu-doped composite coatings, Ag-doped antifouling coatings, and Cu/Ag-co-doped antifouling coatings. Furthermore, it focuses on the quality of coatings in typical case studies, including factors such as coating thickness, adhesion, environmental compatibility, and long-term durability. Finally, the future development of high-strength antifouling coatings is projected, aiming to provide more effective antifouling solutions for the marine engineering field.

2. Preparation Technology of Antifouling Coating

In antifouling coating preparation, recent research focuses on depositing materials with specific properties onto substrates. Advanced techniques are used to enhance antifouling performance, corrosion resistance, and wear resistance. These improvements help substrates adapt to different marine environments. This chapter will discuss the process principles, typical applications, and specific research progress of various coating preparation technologies, including cold spraying, plasma spraying, magnetron sputtering, and laser cladding. Based on the analysis of multiple technologies' process advantages and application status on different materials, suitable preparation technology references are provided for selecting coatings to improve durability.

2.1. Cold Spray

Cold spray is a coating deposition technology with a working temperature range from low to several hundred degrees Celsius (typically below 600 °C). The process involves accelerating solid micron-sized powder particles, such as metals or ceramics, to supersonic speeds using a high-pressure carrier gas like N_2 or He. When these high-speed particles impact the substrate, their substantial kinetic energy causes them to undergo plastic deformation and tightly adhere to the substrate, forming a dense coating. Throughout this process, the particles remain solid rather than melting, thus retaining the material's original

properties, such as electrical conductivity and mechanical strength [48–59]. Compared to traditional thermal spray techniques, cold spray operates at lower temperatures, which prevents the melting of materials and avoids the oxidation and thermal stress issues caused by high temperatures.

Cold spray is widely used in the preparation of antifouling coatings. For instance, Lupoi et al. [60] developed antifouling coatings on organic polymer substrates, Huang et al. [61] produced Cu/Al_2O_3 composite coatings, and Ding et al. [62–64] applied Cu/Cu_2O coatings on steel surfaces. Guo et al. [61] utilized cold spraying technology to prepare Cu/Al_2O_3 composite antifouling coatings on Q235 steel. The coating system consisted of a flame-sprayed Al_2O_3 base layer and a cold-sprayed Cu top layer. The Al_2O_3 layer acted as an insulating barrier to prevent galvanic corrosion between the Cu coating and the steel substrate while ensuring a controlled release of Cu ions to enhance antifouling performance. The sample size was 10 mm × 10 mm, with the Al_2O_3 layer thickness approximately 250 μm and the Cu layer thickness approximately 200 μm. In terms of coating uniformity, cold-sprayed Cu/Al_2O_3 coatings exhibited a dense and homogeneous structure. The adhesion strength between the Cu layer and the Al_2O_3 layer was approximately 10 MPa, and between the Al_2O_3 layer and the steel substrate was about 20 MPa, ensuring good mechanical stability.

Ding et al. [62] utilized cold spray technology to prepare Cu/Cu_2O composite coatings on Q235 steel substrates. The sample size was 150 mm × 150 mm × 3 mm, and the coatings were composed of varying proportions of copper and cuprous oxide (Cu_2O), specifically 0%, 10%, 20%, and 30% Cu_2O. In terms of coating uniformity, the Cu/Cu_2O coatings exhibited a dense structure with low porosity. However, as the Cu_2O content increased, the bond strength of the coatings decreased, with 30% Cu_2O being the upper feasible limit. For adhesion, the cold-sprayed coatings demonstrated high adhesion and mechanical stability, making them suitable for high-velocity water flow environments. Regarding antibacterial performance, tests using diatoms (Navicula pinna, Navicula rows, and Navicula parva) showed that the 30% Cu_2O coating was the most effective in inhibiting diatom attachment, achieving a 100% inhibition rate within 72 h. In terms of long-term stability, the coatings maintained a stable release of copper ions throughout the 30-day seawater immersion test, ensuring sustained antifouling performance. The galvanic interaction between copper and Cu_2O enhanced the electrochemical dissolution of copper, ensuring a consistent ion release rate.

Additionally, there are studies on optimizing the process. C. Stenson et al. [65] used experimental and computational fluid dynamics methods to reveal the effects of cold spray Cu coating processes on coating quality. The research shows that higher nozzle inlet pressure improves particle penetration depth and surface coverage, with the optimal pressure range being 15 to 30 bar. Increasing the pressure beyond this range causes excessively high particle velocities, leading to substrate surface erosion and a reduced coating quality. A slower nozzle scanning speed enhances particle penetration depth, as embedded particles can be further driven into the substrate by subsequent particles. However, increasing the powder feed rate does not significantly improve penetration depth. When the feed rate exceeds 45%, increased particle interaction causes some particles to rebound or accumulate on the substrate surface, limiting further penetration.

The advantage of cold spray technology lies in its low-temperature operation, which prevents material melting, thus preserving the original properties of the materials, such as electrical conductivity and mechanical strength. Cold spray has demonstrated significant potential when applying marine antifouling coatings. However, various process parameters greatly influence coating quality. For example, an appropriate nozzle inlet pressure range and a slower spraying speed can enhance particle penetration depth and surface coverage. However, excessively high pressure or an increased powder feed rate can negatively affect coating quality, leading to substrate surface erosion or particle rebound. Proper control of process parameters is crucial for optimizing cold spray coatings.

Future research can continue to optimize process parameters, improve coating quality, and develop material combinations better suited to different substrates and protection requirements.

2.2. Plasma Spraying

Plasma spraying is a coating technology that uses a plasma arc as a heat source. By creating high-temperature plasma through inert gases between electrodes, powdered materials are heated to a molten or semi-molten state, and these molten particles are then propelled onto the substrate surface using high-pressure gas to form a dense coating. Relying on its high temperature and high-velocity characteristics, the sprayed material impacts the substrate at an extremely high speed, creating a layer that tightly bonds to the substrate [66–76]. Plasma spraying technology has been studied in preparing antifouling coatings [34,35,77–80]. Typical studies include the behavior of Cu-based composite coatings, TiO_2 coatings, etc., in marine pollution prevention.

Tian et al. [79] utilized plasma spraying technology to prepare Cu–Ti composite coatings on Ti-6Al-4V(TC4) alloy substrates. The sample size was 20 mm in diameter by 2 mm in thickness, and the average thickness of the coatings was approximately 300 μm. In terms of coating uniformity, the coatings exhibited dense microstructures with well-bonded Cu and Ti interfaces, along with minimal pores and oxide inclusions. The Cu and Ti layers were uniformly distributed, contributing to the formation of micro-galvanic cells. For adhesion, the coatings demonstrated strong interfacial bonding with the substrate, with an average adhesive strength exceeding 40 megapascals, which was attributed to the effective filling of substrate pores by Cu droplets during the spraying process. In terms of long-term stability, immersion tests in artificial seawater showed that the micro-galvanic structure enabled the uniform release of Cu ions, maintaining high antifouling efficiency throughout the immersion period. This slow-release mechanism, combined with a self-polishing effect, ensured that the coatings provided durable and environmentally friendly antifouling performance.

Researchers have recently studied the combined technology of plasma spraying and laser surface texturing. Yi et al. [35] prepared TiO_2 ceramic coatings through plasma spraying. They compared the performance of coatings with the highest density of micro-scale protrusions to those with fewer groove structures. The coating with the protrusion structure had a larger remelted area, resulting in more anatase TiO_2, a phase with high photocatalytic activity, thereby enhancing the photocatalytic performance of the coating. After 72 h of diatom settlement experiments, the coating showed the smallest fluorescent area, demonstrating superior performance in preventing marine organism attachment. The higher-density microstructure also increased the surface flow velocity, further inhibiting biofouling attachment. In addition, plasma spraying can be used to create coatings with a micron-layered structure, which allows for the controlled release of antifouling elements, thereby extending the coating's antifouling performance and reducing environmental pollution, as will be further analyzed in the next section [81].

Due to the extreme temperatures generated by the plasma arc, this technique is suitable for preparing high-melting-point coating materials, including metals, ceramics, and composites. Additionally, the dense coating structure, with low porosity, effectively prevents the penetration of gases or liquids, making it ideal for high-temperature and highly corrosive environments.

2.3. Magnetron Sputtering

Magnetron sputtering technology is a physical vapor deposition technique commonly used for thin film deposition, utilizing radio frequency and direct current power sources [82–90]. In the magnetron sputtering process, argon gas, an inert gas, is first introduced into the vacuum chamber. Under the electric field applied by the power source (either direct current or radio frequency), the argon gas becomes ionized, generating positively charged argon ions. These ions are accelerated by the electric field and collide with

the target material's surface at high speeds. At the same time, the magnetron system generates a magnetic field in the sputtering region, allowing the charged ions to rotate within the magnetic field. As the ions rotate, their paths are extended, enhancing the ionization process and increasing sputtering efficiency. Under the combined influence of the electric and magnetic fields, the argon ions bombard the target surface, ejecting its atoms, and these atoms travel through the vacuum towards the substrate surface, gradually attaching to it. As the atoms continue to diffuse, accumulate, and bond together, they eventually form a thin film on the substrate with the same composition as the target material.

Research on preparing antifouling coatings using magnetron sputtering technology is ongoing, with coating materials including Cu/graphite-like carbon (GLC) composite coatings, Ti/(Cu, MoS_2) composite coatings, and TiO_2 coatings [91–95]. At the same time, the mechanisms by which magnetron sputtering processes affect coating quality are also being explored.

Wang et al. [95] studied the process of depositing TiO_2 films on 5083 aluminum alloy substrates. The film thickness increased with higher sputtering power, ranging from 248.7 ± 9.3 nm at 6 kW to 554.7 ± 5 nm at 15 kW. At a low power of 3 kW, the film surface was relatively smooth, with a roughness value of 2.269 nm, while at a higher power of 8 kW, the roughness increased to 10.612 nm. The higher power promoted grain growth, resulting in larger surface particles. Increasing the bias voltage enhanced the ion energy, improving the film's density and reducing roughness. On the sample with a roughness of 2.269 nm, *Escherichia coli* (*E. coli*) density was 217 cells/mm^2. In comparison, the bacterial density increased significantly on the sample with a roughness of 10.612 nm. The ratio of oxygen to argon significantly influenced the crystalline phase composition of the TiO_2 films, with a higher oxygen ratio promoting the formation of more oxide phases, thereby enhancing the film's antifouling and anticorrosion properties.

Chen et al. [91] utilized magnetron sputtering technology to prepare CrN-Ag composite coatings on 316 L stainless steel substrates. The coatings were based on a CrN matrix with varying contents of silver (Ag), specifically 4.96 at.%, 8.06 at.%, 13.18 at.%, and 18.37 at.%. The sample size was 30 mm × 30 mm × 2 mm, and the coating thickness ranged from 2.1 to 3.5 μm. In terms of coating uniformity, the CrN-Ag coatings exhibited dense and uniform structures. However, as the silver content increased, agglomeration of silver particles was observed, affecting the microstructure of the coatings. For adhesion, a thin chromium interlayer was introduced during the deposition process to enhance the bonding between the coating and the substrate, ensuring good adhesion and mechanical stability. Regarding antibacterial performance, tests against *Escherichia coli* (*E. coli*) and *Bacillus subtilis* showed that the coating containing 13.18 at.% silver exhibited the best antibacterial effect. The coating achieved a 100% inhibition rate against *Bacillus subtilis* within 6 h and a 100% inhibition rate against *E. coli* within 24 h. In terms of long-term stability, the CrN-Ag coatings demonstrated excellent antifouling performance during a 30-day immersion test in artificial seawater. The attachments of Chlorella, *Nitzschia closterium*, and *Phaeodactylum tricornutum* were reduced by 45%, 72%, and 64%, respectively. The coating with 13.18 at.% silver showed the most significant antifouling effect, maintaining high-efficiency performance over the long term.

Zhang et al. [93] utilized magnetron sputtering technology to prepare Ti/(Cu, MoS_2)-DLC composite coatings on 304 stainless steel substrates. Four types of coatings were prepared: S1 was a DLC coating containing only MoS_2 without Cu; S2 contained 5.3 at.% Cu and MoS_2; S3 contained 7.6 at.% Cu and MoS_2; and S4 contained 9.0 at.% Cu and MoS_2. The sample size was 30 mm × 20 mm × 2 mm, with coating thicknesses ranging from 0.7 μm to 1.6 μm, and the Ti interlayer thickness was approximately 180 nm. In terms of coating uniformity, all samples exhibited dense and uniform microstructures. However, increasing the Cu content led to larger surface particles and a gradual increase in surface roughness, with the roughness of S1 being 2.99 nm, S2 being 4.37 nm, S3 being 7.6 nm, and S4 reaching 10.80 nm. For adhesion performance, the Ti interlayer significantly enhanced the bonding between the coating and the substrate. As Cu content increased, the

critical delamination load improved from 7.4 N (S1) to 19.8 N (S4), demonstrating enhanced mechanical stability.

Magnetron sputtering technology offers considerable flexibility and controllability in preparing antifouling coatings and has advantages in producing thin films. By adjusting process parameters such as sputtering power, bias voltage, and gas ratio, the microstructure and surface characteristics of the coating can be effectively controlled, thus influencing its antifouling performance. However, the impact mechanisms of different material combinations and process conditions on coating performance require further in-depth study. Future research could focus on exploring the preparation of new composite materials and multilayer coatings and understanding the relationship between process parameters and coating performance to develop more efficient and environmentally friendly antifouling solutions.

2.4. Laser Cladding

Laser cladding is a technique for surface modification and additive manufacturing that employs high-density laser beams to fuse powder materials, which then rapidly solidify on the substrate. This results in a compact layer that metallurgically integrates with the underlying material [96–104]. In preparing antifouling coatings, research on laser cladding mainly focuses on fabricating metal-based coatings, such as Cu-Cr, Cu-Mn, Cu-Fe, and high-entropy alloy coatings [42,105,106].

Ma et al. [42] utilized laser cladding technology to prepare Cu-Fe composite coatings on steel substrates and evaluated their antifouling performance in marine environments. The coatings had a thickness of 350 μm, and experiments were conducted with 8%, 12%, and 16% Cu content. Through rapid cooling, the coatings formed a dense structure, preventing segregation and porosity, with Cu-rich matrix phases and Fe precipitates uniformly distributed. The Fe precipitates appeared as spherical particles with diameters of 500–1000 nanometers. The coatings demonstrated excellent adhesion, which was further enhanced by the microchannel structures formed through dealloying, improving the mechanical bonding between the coatings and the substrate. Tests showed that the $Fe_{12}Cu$ coating achieved a stable copper ion release rate within 15 days, effectively inhibiting the attachment of marine organisms. During a 30-day seawater immersion test, the coatings exhibited outstanding self-polishing performance, reducing the accumulation of corrosion products and biofouling. The antifouling lifespan of the $Fe_{12}Cu$ coating was predicted to reach 25 years, significantly exceeding the 3–5 year lifespan of traditional coatings. The 12% Cu content ($Fe_{12}Cu$ coating) was identified as the optimal combination.

Verma et al. [105] utilized laser cladding technology to deposit CoCrFeNi and CoCrCuFeNi high-entropy alloy coatings on Indian naval steel (DMR 249A) substrates. The sample size was 300 mm × 300 mm × 30 mm. The thickness of the CoCrFeNi coating was approximately 830 μm, while the CoCrCuFeNi coating was approximately 630 μm. In terms of coating uniformity, both coatings exhibited dense microstructures without any cracks. The Cu in the CoCrCuFeNi coating segregated as a second FCC phase. For adhesion, the coatings formed metallurgical bonds with the substrate, ensuring good interfacial stability. Regarding antibacterial performance, antibacterial tests using *Escherichia coli* (*E. coli*) showed that the CoCrCuFeNi coating reduced bacterial growth by 88%, significantly outperforming both the CoCrFeNi coating and the DMR 249A substrate. This performance was attributed to the release of Cu ions from the CoCrCuFeNi coating, which effectively killed bacterial colonies.

Laser cladding technology is gaining attention in preparing antifouling coatings due to its high precision, controllability, and environmental friendliness. Compared to magnetron sputtering, it enables the production of thicker coatings. In the field of antifouling coating preparation, optimizing laser processing parameters has enabled the refinement of microchannels within the coating, thereby achieving control over the release rates of antifouling ions. However, the impact mechanisms of different materials and elemental distributions on the formation of microchannels and their antifouling effects still require further investigation. Future research can focus on developing more complex multi-element

alloy systems and further exploring the relationship between process parameters and microstructure control to achieve more efficient and long-lasting antifouling effects.

2.5. Micro-Arc Oxidation

Micro-arc oxidation (MAO) is a technology that forms an oxide ceramic layer on the surface of metal materials through electrochemical methods [107–115]. By applying high voltage in the electrolyte, micro-discharges occur on the metal surface, forming an oxide layer that is wear-resistant, corrosion-resistant, and thermally stable. Zhang et al. [116] prepared a Cu-doped TiO_2 composite coating using MAO, with 10 g/L Na2Cu-EDTA as the copper ion source, resulting in a dual-layer structure. Based on the characteristics of MAO, the inner layer, formed under low discharge density and rapid cooling, produced a dense TiO_2 layer, providing adhesion and corrosion resistance, preventing the penetration of corrosive media. The outer layer, subjected to high-temperature melting and rapid cooling, developed a porous structure, increasing the surface area and offering channels for the sustained release of copper ions. The study revealed regional variations in copper content within the coating: the high-copper-content area, with 4.2 wt% copper, primarily contained CuO, exhibiting stronger antibacterial performance, while the low-copper-content area, with 2.3 wt% copper, mainly consisted of Cu_2O, with relatively weaker antibacterial effects. Copper ion release tests indicated that the high-copper-content area had a release rate of 8.1 ppb/cm^2, higher than the 3.3 ppb/cm^2 of the low-copper-content area. In antibacterial tests against *Staphylococcus aureus*, the high-copper-content area showed a higher bacterial mortality rate, with SEM observations revealing significant bacterial membrane rupture, whereas only minor deformation was observed in the low-copper-content area.

Micro-arc oxidation and ultrasonic vibration were used by Hu et al. to prepare Cu-doped titanium dioxide coatings [117]. The introduction of ultrasonic waves enhanced the incorporation of Cu into the coating, increasing the coating thickness from 8.1–12.8 μm to 13.5–26.2 μm while reducing the porosity from 4.85% to 4.03%. In a 14-day sulfate-reducing bacteria culture experiment, the untreated titanium surface exhibited a large amount of bacterial and biofilm attachment, showing poor antifouling performance. In contrast, the Cu-doped titanium dioxide coating, with a Cu content of 2.13%, significantly reduced microbial attachment on the surface, and the bacterial cell membranes were ruptured, demonstrating a marked bactericidal effect. On this coating, bacterial attachment was decreased by more than 80% compared to untreated titanium, and biofilm coverage was reduced, showing notable antifouling properties.

MAO has gained widespread attention in the preparation of antifouling coatings due to its high adhesion, excellent corrosion resistance, and antibacterial properties, along with its environmentally friendly and easily controllable process. Compared to other surface modification techniques, MAO coatings feature a thicker and more porous structure, which not only enhances the surface area of the coating but also provides channels for the sustained release of antibacterial ions or antifouling agents. In the development of antifouling coatings, optimizing MAO process parameters can further regulate the microstructure of the pores, enabling precise control over the release rates of antibacterial ions. However, the mechanisms by which different materials and elemental distributions influence the formation of microstructures and their antifouling performance require further investigation. Future research could focus on developing complex multi-element doping systems and exploring the relationship between process parameters and microstructure control to achieve more efficient and long-lasting antibacterial and antifouling effects.

2.6. Other Technology

In addition to the techniques above in antifouling coating research, there have also been studies involving high-velocity oxygen fuel (HVOF), spark plasma sintering (SPS), and pulsed electrospark deposition (PED).

SPS is an advanced sintering technique that applies pulsed direct current (DC) through a powder compact while simultaneously applying uniaxial pressure. The rapid heating gen-

erated by the electric current and the applied pressure allows for fast sintering at relatively low temperatures, reducing grain growth and preserving the material's nanostructure. This process enables the production of high-density, nanocrystalline materials and composite materials, with improved mechanical properties and uniform microstructures [118–120]. The key advantages of SPS include short processing times, high precision, and the ability to sinter materials with complex compositions that are challenging for conventional sintering methods. In studies using traditional casting methods to prepare Al 0.4CoCrFeNiCu high-entropy alloys [121], it was found that Cu plays a positive role in the antifouling performance of the coating. Still, Cu segregation reduces the alloy's corrosion resistance and strength. Yu et al. [122] used the SPS technique to sinter AlCoCrFeNiCu0.5 alloys under high pressure (30 MPa) and high temperature (1423 K) in a vacuum environment, discovering that Cu could dissolve uniformly into the high entropy alloy matrix without large-scale segregation with other elements. The alloy's antifouling performance in marine environments improved; electrochemical impedance increased; and it exhibited higher yield strength (1203 MPa), fracture strength (2447 MPa), and plastic strain (26.37%). The results confirmed that the use of SPS can alter the form of Cu in the alloy, thereby improving the comprehensive properties of the alloy, including antifouling, corrosion resistance, and mechanical performance.

HVOF is a thermal spray process in which a combustion gas mixture is ignited and passed through a nozzle at high speeds [123–129]. The combustion produces a high-temperature, high-pressure gas stream that accelerates the coating particles to supersonic velocities. Upon impact with the substrate, the molten or semi-molten particles rapidly solidify, forming a dense, well-adhered coating. The high velocity minimizes the porosity and oxidation of the coating material, resulting in strong adhesion, excellent mechanical properties, and corrosion resistance. HVOF coatings are widely used in environments requiring wear resistance and thermal protection, such as marine equipment and turbine components. Piola et al. [34] studied the comparison of antifouling performance between HVOF coatings and traditional atmospheric plasma spraying ceramic coatings in marine hydraulic applications. The sample size was 25 mm × 50 mm × 6 mm. In terms of coating uniformity, the HVOF coatings exhibited low porosity and high uniformity, with the dense structure effectively reducing defects and preventing fouling attachment. For adhesion, the HVOF coatings formed strong metallurgical bonds with the substrate. In terms of long-term stability, after 20 weeks of marine exposure experiments, the fouling coverage of HVOF coatings was lower than that of APS coatings. Mainly in tropical environments, the fouling coverage of HVOF coatings was below 20%, while that of APS coatings was close to 90%. The HVOF coatings demonstrated excellent durability throughout the testing process Additionally, the surface roughness (Ra) of HVOF coatings was low, ranging from 0.06 to 0.10 μm, while the surface roughness of APS coatings was 0.26 μm.

PED is a surface modification technique that enhances materials by depositing electrode material onto a substrate via high-frequency pulsed discharges. It generates localized high temperatures, transforming the material into plasma that fuses onto the surface. PED provides process flexibility and precise control over coating thickness and roughness, ensuring uniform chemical incorporation [130–134]. E.I. Zamulaeva et al. [135] prepared Ag-doped multicomponent coatings on Grade 4 titanium using PED and ion implantation techniques. Composite electrodes, with Ag content ranging from 0 to 2.0 at%, were fabricated through the self-propagating high-temperature synthesis method. The sample dimensions were 15 mm × 15 mm × 3 mm, with the coatings having an average thickness of 30 μm. The study revealed that all coatings contained TiC particles, a titanium matrix, and CaO and MgO oxides. However, as the Ag content increased, the size of TiC particles decreased, and the Ag particles became more uniformly distributed with higher density. In coatings with higher Ag content (2.0 at%), the formation of an Ag-Mg solid solution phase was also observed. Moreover, Ag doping significantly enhanced the antibacterial properties of the coatings. All Ag-doped coatings exhibited 100% antibacterial activity against both Gram-positive *Staphylococcus aureus* and Gram-negative *Escherichia coli* within 24 h,

with Ag content between 0.5 and 1 at% being sufficient to achieve effective antibacterial performance.

A.N. Sheveyko et al. [131] prepared Ag-doped coatings on titanium-based materials using PED and analyzed the effects of different deposition environments—argon, water, and air—on the coatings' performance. The coatings had a thickness of 30 μm, with surface roughness (Ra) ranging from 3.7 to 6.1 μm. The coating deposited in the argon environment exhibited the highest hardness, reaching 11 GPa, primarily due to the high TiC phase content, which enhanced its mechanical properties and wear resistance. Additionally, the dense structure formed under this environment minimized oxidation reactions, improving the mechanical stability of the material. In the water environment, oxidation reactions on the coating surface intensified, resulting in the formation of more oxides. This led to an increased release rate of Ag+ ions, with a concentration of 480 ppb within five days, which significantly enhanced antibacterial performance but potentially compromised long-term structural stability. In contrast, the air environment produced milder oxidation reactions, with a lower Ag+ ion release concentration of 140 ppb. While the coating under air conditions maintained better chemical stability, its antibacterial performance was weaker compared to the water-deposited coating.

Although these technologies hold potential for antifouling coating preparation, they also have certain limitations. For example, micro-arc oxidation faces challenges in controlling coating thickness and uniformity, HVOF spraying may lead to high-temperature oxidation, and SPS is costly and requires complex equipment. The long-term stability and durability of these technologies in marine environments also require further optimization and validation. Future research can explore optimizing the process parameters of these technologies to enhance the antifouling performance of the coatings.

Table 1 summarizes the typical research results on the preparation technologies of antifouling coatings, including the substrate and coating compositions, component dimensions, coating uniformity, adhesion, and antifouling stability. Different deposition techniques demonstrate specific potential in their respective marine antifouling applications.

The primary advantage of cold spray technology lies in its low-temperature operation, which prevents material melting and retains the material's original properties, such as electrical conductivity and mechanical strength. It is suitable for the preparation of heat-sensitive and easily oxidized metal coatings. This makes it applicable in the field of marine antifouling equipment for precision components that require protection from thermal damage, such as sensors and other electronic surfaces. However, since cold spray coatings do not form metallurgical bonds, their adhesion is generally lower than that of techniques like laser cladding. For example, as shown in the study by Guo et al. [61], the adhesion between Cu and the intermediate Al_2O_3 layer was 10 MPa. The cost of cold spray primarily depends on the type of substrate and coating materials, followed by the cost of using high-pressure gases. Compared to energy-intensive and high-manufacturing-cost processes such as magnetron sputtering and laser cladding, cold spray offers a cost advantage.

Plasma spraying technology can handle high-melting-point metals, ceramics, and composites, producing dense and low-porosity coatings that prevent gas and liquid penetration. This makes it a suitable choice for equipment components used in high-temperature and corrosive environments, such as marine and chemical equipment. The cost of plasma spraying is primarily determined by the energy consumption required for high-temperature operations, equipment maintenance, and the price of the materials used.

Magnetron sputtering technology offers some flexibility and controllability in producing antifouling coatings, particularly thin film coatings. In the marine antifouling sector, it is mainly used for depositing thin films on electronic equipment. However, due to the limited thickness of the films, magnetron sputtering is not suitable for applications requiring wear resistance. The cost of this technology depends on the price of the sputtering targets and the complexity of the process control, and it is also influenced by the number and types of materials used in the coatings. Overall, the cost of magnetron sputtering is higher than that of cold spray technology.

Table 1. Summary of deposition methods and their characteristics.

Deposition Method	Materials	Dimensions	Uniformity	Adhesion	Stability
Cold spray	Substrate: Q235 carbon steel Coating: Al_2O_3 base layer with Cu top layer [61]	Sample size: 10 mm × 10 mm Layer thickness: Al_2O_3: 250 μm; Cu: 200 μm	Dense, homogeneous	10 MPa (Cu to Al_2O_3); 20 MPa (Al_2O_3 to steel)	Stable during 30-day seawater test
	Substrate: Q235 carbon steel Coating: Cu/Cu_2O composite (0%, 10%, 20%, 30% Cu_2O) [62]	Sample size: 150 mm × 150 mm × 3 mm Layer thickness: Varies with Cu_2O content	Low porosity; uniformity decreases with >30% Cu_2O	-	-
Plasma spraying	Substrate: TC4 alloy Coating: Cu-Ti composite coatings [79]	Sample size: 20 mm diameter Layer thickness: 300 μm	Dense with minimal pores	Exceeds 40 MPa	-
Magnetron sputtering	Substrate: 5083 alloy Coating: TiO_2 thin films [95]	Sample size: 248–554 nm Layer thickness: 248–554 nm	-	-	Stable during 30-day seawater test
	Substrate: 316L stainless steel Coating: CrN-Ag composite coatings with varying Ag contents [91]	Sample size: 30 mm × 30 mm × 2 mm Layer thickness: 2.1–3.5 μm	Dense but with Ag particle agglomeration at high content	-	Stable during 30-day seawater test
Laser cladding	Substrate: steel substrate Coating: Cu-Fe composite (8%, 12%, 16% Cu content) [42]	Sample size: 300 mm × 300 mm × 30 mm Layer thickness: 350 μm	Dense structure with evenly distributed phases	Metallurgical bonding	Antifouling lifespan of 25 years
	Substrate: DMR 249A steel Coating: CoCrCuFeNi high-entropy alloy	Sample size: 300 mm × 300 mm × 30 mm Layer thickness: 630–830 μm	-	Metallurgical bonding	Durable coating for long-term use
Micro-arc oxidation	Substrate: titanium Coating: Cu-doped TiO_2 composite coatings [105]	-	Porous outer layer with dense inner structure	High adhesion through oxide layer formation	-

Micro-arc oxidation technology in marine antifouling research primarily focuses on the preparation of porous ceramic layer coatings. With an intermediate layer, it can form good adhesion with the substrate and is suitable for specific material requirements in equipment components. The cost of MAO mainly depends on energy consumption and the type of substrate used, though it generally remains lower compared to other deposition techniques.

Laser cladding technology is characterized by the production of thick coatings with metallurgical bonding, as shown in the research by Ma et al. [42]. It is suitable for large-scale components and high-load environments, such as marine engineering equipment. Its thick coatings provide excellent wear resistance and antifouling performance. However,

the high cost of laser cladding is mainly determined by equipment maintenance, energy consumption, and the price of the coating materials used.

3. Progress in Marine Anti-Fouling Coatings

As research into marine anti-fouling coatings advances, different coatings have been developed and applied, with Cu-doped and Ag-doped coatings standing out due to their notable antimicrobial properties. Both Cu and Ag exhibit strong antifouling effects by effectively disrupting the cellular structures of marine organisms, thereby preventing biofouling. The following sections will delve into recent developments and applications of Cu-doped and Ag-doped antifouling coatings, aiming to provide a reference for future studies and practical applications.

3.1. Cu-Doped Antifouling Coating

Cu as an antifouling material can be traced back to the Phoenicians and Carthaginians in 700 BC when Cu sheathing was used to prevent biofouling and pollution on ship hulls [136]. By the mid-19th century, the Liverpool dockyards in England began using Cu sulfate in their antifouling paints [136]. Entering the 20th century, tributyltin (TBT) became the new standard for antifouling due to its effective properties. However, due to environmental concerns, many countries began banning its use in the 1980s, and the International Maritime Organization prohibited TBT paints in 2008 [137,138]. Subsequently, Cu-based antifouling paints gradually regained attention, among which Cu-doped polymer coatings, valued for their ease of use and low cost, have seen widespread application.

Under specific working conditions, antifouling coatings must possess a certain surface strength level. Therefore, metal-based antifouling coatings are also an important research direction. In the 1990s, Japan's Nisshin Steel Co. developed three Cu-containing NSS-AM antibacterial stainless steels [139,140]. The alloys possess corrosion resistance, wear resistance, and mechanical properties while exhibiting antibacterial performance. Further investigations by other researchers [141] have also confirmed that adding an appropriate amount of Cu to stainless steel can produce a bactericidal rate of approximately 99% against *Escherichia coli*, *Staphylococcus aureus*, and yeast.

Additionally, studies have shown that the ε-Cu antibacterial phase is crucial, as it damages bacterial cell walls and membranes, causing leakage of intracellular fluids. This disruption of metabolic processes ultimately leads to cell death, providing antibacterial effects [142–145]. This type of antibacterial stainless steel has been applied in the food industry and medical devices. Research on Cu-containing metal-based coatings for marine antifouling has gradually emerged, focusing on Cu-Fe coatings, Cu-Cr coatings, Cu-Ti coatings, and Cu-containing high-entropy alloy coatings.

3.1.1. Cu-Doped Polymer Coatings

In Cu-doped polymer coatings, the polymer matrix provides specific adhesion and mechanical properties, and the antifouling effect is achieved by controlling the release of Cu ions.

Research on the effects of three polyurethane-based antifoulings, International Paint Trilux 33 (AF), International Paint Micron Extra 2 (CDP), and International Paint Micron 77 (SPC), on the corrosion and biofouling of aluminum substrates revealed that the corrosion behavior of the coatings influences their antifouling performance [146]. When Cu in the coatings comes into direct contact with the aluminum substrate, electrochemical corrosion is induced. Among the tested formulations, CDP and SPC, with higher Cu oxide content, exhibit faster corrosion rates. CDP contains Cu oxide and zinc oxide as the main antifouling components, while SPC includes Cu oxide and Cu pyrithione. Both present a higher corrosion risk for aluminum due to their elevated Cu oxide content.

On the other hand, AF uses Cu thiocyanate as the active ingredient, with lower Cu content, resulting in less severe corrosion. Controlling active ingredient release can produce antifouling effects in polymer-based antifouling coatings. However, it is important to

consider the compatibility between the coating's composition and the substrate to minimize the risk of electrochemical corrosion

The state of Cu affects its antifouling ability [147,148]. In studies on the metal release and impact of Cu-doped epoxy resin coatings on marine sessile invertebrate communities, it was found that nano-Cu coatings exhibit more robust antifouling capabilities, as they can more efficiently release Cu ions, thereby inhibiting biofouling [149]. In contrast, the antifouling performance of non-nano Cu-doped epoxy resin coatings is weaker, with slower release rates, and over time, some Cu may precipitate in particulate form, reducing the release of effective Cu ions. The differences in release rates can be attributed to several factors. The larger specific surface area of nano-Cu allows for a more rapid release of copper ions. Compared to non-nano Cu, nano-Cu has smaller particle size and larger surface area, which increases the opportunities for its surface to interact with the environment, thereby accelerating the release of ions. Active chemical potential also plays an important role. In nano-Cu coatings, the unique surface characteristics and higher energy state may result in the released copper ions having a higher active chemical potential. This means that, under the same chemical environment, nano-Cu is more likely to release copper ions than non-nano Cu.

Robert J et al. [149] used fiberglass-reinforced plastic plates as substrates to compare the performance of antifouling coatings with nano-scale and non-nano-scale Cu additives. In seawater, the concentration of dissolved Cu in the non-nano Cu coating rapidly peaks within 24 h and then stabilizes. However, in estuarine water, the release of dissolved Cu is slower, reaching its peak only after 72 h, accompanied by an increase in particulate Cu. As for the nano-Cu coating, it primarily releases dissolved Cu in both seawater and estuarine water, with only a minor release of nano-particulates. Although the release of nano-particulates increases slightly in estuarine water, the overall proportion remains low. These results highlight the influence of environmental conditions on Cu release behavior and reveal distinct differences between nano and non-nano Cu-doped epoxy resin coatings.

The loading and release forms of copper play a crucial role in the antifouling performance of the coating. Ding et al. [150] developed a microcapsule-structured antifouling coating by encapsulating Cu_2O particles within the amphiphilic block copolymer PLMA(hydrophobic segment)-b-PDMAEMA(hydrophilic segment), forming a microcapsule structure with Cu_2O as the core and PLMA as the outer layer, as shown in Figure 1a. The coating was applied to Q235 steel plates as the substrate, with the plates measuring 150 mm × 150 mm × 3 mm. Figure 1b illustrates the antifouling mechanism of the coating: Cu_2O acts as the active component, gradually releasing copper ions upon contact with seawater to achieve antifouling effects. The outer layer, composed of hydrophobic PLMA chains, allows Cu_2O particles to be evenly dispersed within the resin matrix, enhancing the overall stability of the coating. Additionally, the PDMAEMA chains coordinate with copper ions to control the release rate of Cu^{2+}, ensuring the coating delivers long-lasting antifouling performance.

Comparative studies show that while Cu_2O powder exhibits a higher copper ion release rate, it is unstable: the release rate decreases to 1.52 μg/(mL·d) after one week, further dropping to 0.51 μg/(mL·d) after three weeks, and slowing to 0.15 μg/(mL·d) by the eighth week. In contrast, the Cu_2O coating embedded within the PLMA-b-PDMAEMA copolymer maintains a stable concentration over 17 weeks, demonstrating a more consistent copper ion release, ensuring long-lasting antibacterial performance. Antibacterial tests reveal that the PLMA-b-PDMAEMA copolymer coating effectively inhibits both Gram-positive and Gram-negative bacteria, with the 2:1 ratio of PLMA to (hydrophilic segment) achieving the most pronounced antibacterial effect.

The EIS test analyzed the corrosion resistance of the Cu/Cu_2O coating, and the results showed that the impedance modulus of the coating increased with the Cu_2O content. The coating containing 30% Cu_2O exhibited the highest impedance modulus at low frequency (0.01 Hz), reaching approximately 1.2×10^5 Ω·cm^2, indicating the best corrosion resistance. In contrast, the coating with 0% Cu_2O had the lowest impedance modulus, only about

2.5×10^3 Ω·cm^2. This demonstrates that increasing the Cu_2O content effectively enhances the electrochemical stability of the coating.

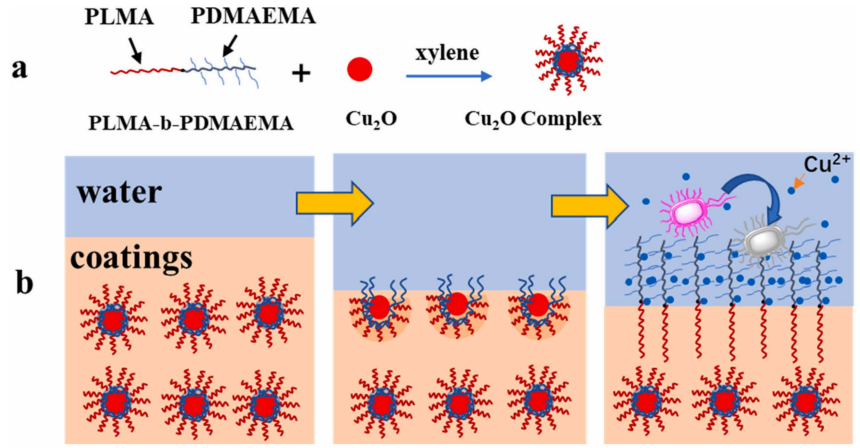

Figure 1. Construction of Cu_2O microcapsules (**a**) and the antifouling process of Cu_2O/PLMA-b-PDMAEMA/PCL coatings in marine environments (**b**) [150].

Studies have shown that composite coatings doped with Cu and other active molecules can also achieve antifouling effects. Liu et al. [26] developed a ZnS:Cu/PDMS composite coating for marine antifouling. Figure 2 illustrates the antifouling mechanism of the coating: Cu acts as an antimicrobial component, inhibiting microbial growth, while Cu-doped ZnS modifies the material's conductivity and band structure, promoting electron–hole pair separation and enhancing Zn^{2+} ion release. The continuous release of Zn^{2+} ions further prevents biofouling. Additionally, the fluorescence properties of ZnS influence microbial phototaxis or disrupt physiological processes, thereby inhibiting biofilm formation. These synergistic mechanisms work together to enhance the coating's antifouling performance.

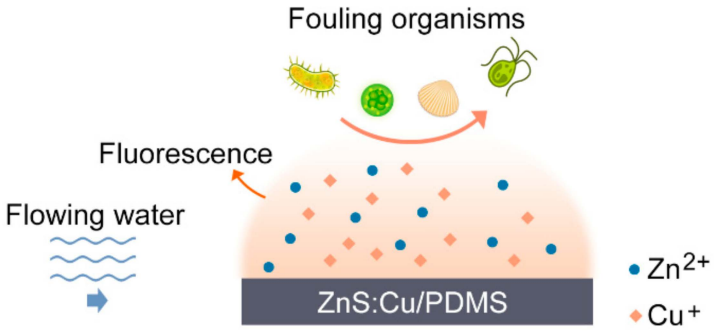

Figure 2. Antifouling mechanism of ZnS:Cu/PDMS composite coating [26].

The results indicate that under static conditions, coatings without ZnS accumulated significant Chlorella growth, while those with 20 wt% and 50 wt% ZnS exhibited minimal attachment. In dynamic environments, the antifouling performance improved, particularly with the 50 wt% ZnS coating, as high ZnS release and surface deformation effectively reduced Chlorella attachment. These findings suggest that increasing ZnS content enhances antifouling performance, especially under dynamic conditions, and that combining multiple antimicrobial components can further improve the effectiveness of the coating.

Cu-doped polymer coatings are widely used in antifouling applications. However, their main drawback is the thinness of the coatings, making them susceptible to damage from mechanical impact and abrasion, especially in harsh marine environments where water flow and particles exacerbate wear, limiting their durability. Therefore, improving mechanical strength and durability while maintaining antifouling performance remains an important direction for future research. Future studies could explore incorporating

other high-strength materials, such as nanomaterials or inorganic fillers, or improving the polymer matrix to enhance the overall performance of the coatings. Additionally, combining polymers with other durable materials could improve their impact resistance and wear durability.

3.1.2. Cu-Containing Metal-Based Coatings

Compared to Cu-doped polymer coatings, Cu-based metal coatings have higher mechanical strength and wear resistance and can achieve antifouling effects through the stable release of Cu ions. However, alloy design and structural optimization are necessary to enhance coating performance since Cu tends to form corrosion products in marine environments, affecting the ion release rate and antifouling durability. This section will discuss several typical Cu-based alloy coatings, including Cu-Fe, Cu-Cr, Cu-Ti, and high-entropy alloy coatings, analyzing their antifouling mechanisms and application performance.

1. Cu-Fe alloy coating

In Cu-based metal coatings, the release of Cu can be regulated by adding a more electropositive metal element to the coating, utilizing the galvanic corrosion properties to control Cu ion release. Researchers have studied the addition of Fe to optimize the Cu release process and enhance antifouling performance. Ma et al. [42] studied Cu-Fe alloy laser cladding coatings with different Fe contents (8 wt%, 12 wt%, and 16 wt%) in a simulated seawater environment, mainly analyzing their corrosion behavior, Cu ion release rates, and antifouling performance. The substrate was Grade 45 steel.

The study showed that adding Fe to the coating formed a galvanic corrosion mechanism, where the Fe phase acted as the anode and preferentially dissolved, forming microchannel structures. These channels promoted the release of Cu ions, enhancing the coating's antifouling effect. As illustrated in Figure 3a, the Cu-Fe coating original model shows a well-structured interface before the corrosion process begins. Upon the dissolution of Fe ions, as depicted in Figure 3b, many small channels were formed within the layer, which allowed seawater and oxygen to penetrate the coating further, accelerating the release of Cu and the overall corrosion process. This ion dissolution led to the formation of porous structures within the coating. Subsequently, as shown in Figure 3c, atomic structure rearrangement occurred, which contributed to changes in the coating's stability over time. Regarding Cu ion release rates, the coating with 12 wt% Fe exhibited the best performance, with 40 $\mu g/cm^2/day$, maintaining stability over 180 days, effectively preventing the attachment of marine microorganisms. In contrast, the coating with eight wt% Fe had a more porous structure and a lower Cu ion release rate. In comparison, the coating with 16 wt% Fe, despite a faster initial Cu ion release, saw a decline in long-term antifouling performance due to the excessively high release rate.

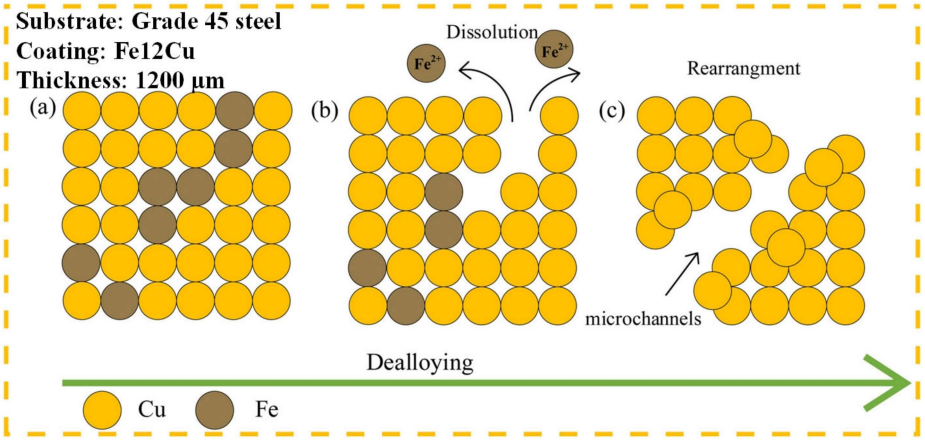

Figure 3. The dealloying mechanism in the Cu-Fe coating [42]. (**a**) Cu-Fe coating original model. (**b**) Fe^{2+} dissolution. (**c**) Atomic structure rearrangement.

Zhao et al. [39] prepared 304L-Cu SS coatings on the surface of 4 mm thick 316L stainless steel sheets. The coating exhibited an adhesion strength of 69 MPa, with a dense microstructure and a porosity of only 0.34%. Elec Performance tests showed that the controlled release of copper ions provided a self-polishing effect, effectively inhibiting the attachment of biofouling organisms such as *Pseudomonas aeruginosa* and *Navicula incerta*. The coating achieved a bacterial inhibition rate of 99.9% and successfully prevented algae accumulation after 7 days of immersion.

Polarization tests revealed that the corrosion behavior of the 304L-Cu stainless steel (SS) coating in artificial exhibited typical active–passive–pitting characteristics. Compared to the uncoated 304L-Cu SS, the passivation zone current density of the coating increased significantly, indicating that although the coating retained the ability to form a passivation film, its corrosion resistance was reduced due to plastic deformation, martensitic transformation, and pore formation. Additionally, the pitting potential decreased from 257.7 mV to 26.3 mV, reflecting a diminished resistance to pitting corrosion. EIS tests further revealed a reduction in the impedance arc diameter for the coated sample compared to the uncoated 304L-Cu SS. In the equivalent circuit model, the protective resistance of the 304L-Cu SS coating decreased from 43,250 $\Omega \cdot cm^2$ to 2693 $\Omega \cdot cm^2$. Although the corrosion resistance of the coating declined, the presence of the passivation film ensured a controlled release of antifouling agents during service, preventing excessive release that could lead to marine pollution.

Additionally, the periodic release of copper ions, combined with the exposure of new surfaces during wear, ensured long-term antifouling performance. Figure 4 illustrates the dynamic evolution of the coating during use. In the first stage, physical wear and corrosion from contact with the marine environment caused localized degradation, exposing new surfaces. In the second stage, these newly exposed surfaces released the embedded copper components into the environment, maintaining the antifouling effect. The third stage involves a self-repair and re-release cycle, where the excellent wear resistance and adhesion of the 304L-Cu SS coating allow degraded areas to partially repair themselves, initiating a new antifouling cycle. This cyclical process ensures that the coating maintains stable antifouling performance over long-term use.

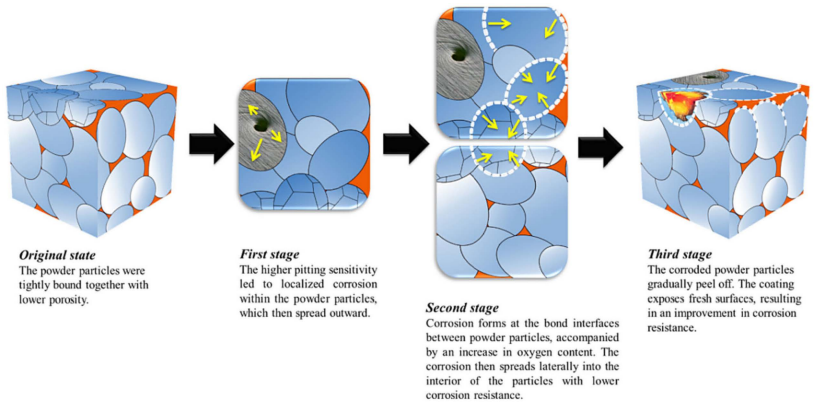

Figure 4. Schematic representation of the surface morphology evolution of the 304L-Cu SS coating [39].

2. Cu-Ti alloy coating

In addition to the Cu-Fe alloy coatings studied for regulating Cu ion release, researchers have also developed Cu-Ti alloy coatings. The principle behind this is that Ti has a higher electrode potential than Cu. Cu acts as the anode when the Cu-Ti coating is in a seawater environment, while Ti is the cathode. Cu ions are slowly and evenly released through the mechanism of micro-galvanic cells, achieving long-lasting antifouling performance. Tian et al. [79] designed alternating layers of Cu and Ti with different ratios (specific Cu contents were 8.1%, 12.8%, 19.2%, 34.5%, 48.6%, and 65.2%) and used APS

to deposit the coatings on TC4 substrates. Antifouling performance tests showed that as the Cu content increased, the antifouling efficiency of the coating significantly improved, reaching nearly 100% when the Cu content exceeded 19.2%.

Figure 5 illustrates the antifouling principle of the alternating layers of Cu and Ti. The micron-scale layered structure forms multiple small micro-galvanic cells within the coating, and as the Cu increases, the number of these micro-galvanic cells also increases. When the Cu content is low, the anode area of each micro-galvanic cell is small, leading to higher current density, which accelerates the dissolution of the anode. Conversely, the anode area becomes relatively larger as the Cu content increases, reducing current density and slowing the dissolution rate. Therefore, coatings with higher Cu content exhibit better antifouling performance. Additionally, as the Cu dissolves, the Ti layers gradually become exposed. The Ti layers are removed by seawater flow, exposing new Cu and Ti layers, forming new micro-galvanic cells, and achieving a self-polishing effect.

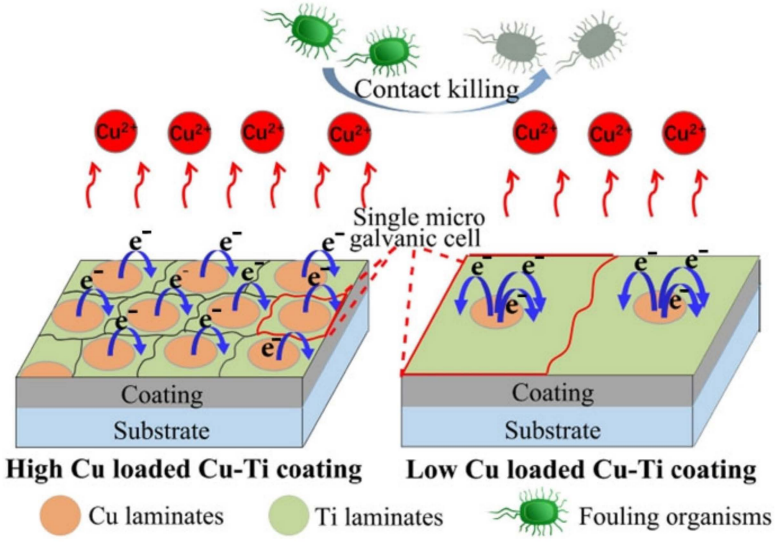

Figure 5. Schematic diagram of the Cu-Ti composite coating [79].

The nanostructured layered architecture in antifouling coatings enhances antifouling performance because it provides a larger specific surface area, increasing the contact area between the coating and seawater, thereby enhancing reaction efficiency. Additionally, the size and surface characteristics of nanoparticles lead to higher reactivity in electrochemical reactions, allowing for a faster release of copper ions and improved antifouling efficacy. Nanoparticles also contribute to a more uniform coating, reducing defects and enhancing overall performance. Furthermore, this layered structure creates more micro-galvanic cells, facilitating a more effective self-polishing effect that continuously releases copper ions to resist biofouling. Lastly, nanostructured coatings can improve corrosion resistance, extending their service life and maintaining long-lasting antifouling properties.

Corrosion test results revealed that the corrosion resistance of Cu-Ti composite coatings varied with the increase in copper content. As the copper content increased from 8.1% to 65.2%, the corrosion potential rose from −327 mV to −232 mV, indicating that higher copper content promoted micro-galvanic corrosion. The corrosion current density also increased with the copper content, rising from 11.82 $\mu A/cm^2$ to 29.91 $\mu A/cm^2$, reflecting a significant enhancement in the dissolution rate. Additionally, the charge transfer resistance decreased from 2706 $\Omega \cdot cm^2$ to 1526 $\Omega \cdot cm^2$, further confirming the reduction in corrosion resistance with higher copper content. Although the dissolution rate of individual micro-galvanic cells decreased, the increased copper content led to a higher number of micro-galvanic cells in the coating, resulting in an overall increase in the dissolution rate.

Under this alternating Cu-Ti coating structure, the 65.2% Cu-Ti coating shows the highest copper ion release rate of 30 $\mu g/(cm^2 \cdot day)$, while the 8.1% Cu-Ti coating has a

maximum release rate of 10.6 μg/(cm^2·day). Compared to Cu/Ti coatings without the micron-scale alternating structure [78], the copper ion release rate is lower, avoiding the excessively rapid ion release seen in traditional coatings. As the Cu content increases from 8.1% to 65.2%, the antifouling lifespan of the coating extends from 4 years to 14 years, indicating that this structured coating offers enhanced antifouling stability.

3. Cu-Cr alloy coatings

Cu-based materials inhibit the attachment of organisms by releasing Cu ions. However, over time, corrosion products such as $Cu_2(OH)_3Cl$ reduce the release of Cu, leading to a significant decline in antifouling performance. Researchers applied laser cladding technology to fabricate Cu-based coatings containing 1%, 3%, and 5% Cr to explore the influence of Cr [151]. As the Cr content increases, Cr-rich phases in the coating form Cr_2O_3 particles during the corrosion process. These particles become embedded in the corrosion products, increasing the internal stress within the corrosion layer leading to cracks and flaking. This exposes more of the coating surface, enhancing the continuous release of Cu ions.

After 180 days, it was revealed that the antifouling performance of coatings with different Cr contents improved significantly as the Cr content increased. The coating containing 5% Cr exhibited the best antifouling performance, with its Cu ion release rate stabilizing above 40 μg/cm^2/d, and the microorganism coverage rate was as low as 3.21%, significantly outperforming the pure Cu coating. The microalgae coverage on the 5% Cr coating was less than 2%, whereas it exceeded 40% on the pure Cu material. Additionally, the introduction of Cr facilitated the flaking of the corrosion product $Cu_2(OH)_3Cl$, which helped maintain the coating's long-term antifouling stability. This study provides theoretical support for optimizing the design and application of Cu-Cr alloy coatings.

It is worth noting that in marine antifouling coatings, Cr is introduced in certain alloys or composite coatings to enhance corrosion resistance and mechanical performance. However, the use of Cr also raises environmental concerns for marine ecosystems. Hexavalent Cr(VI) is a highly toxic substance with strong carcinogenic and mutagenic properties, and it exhibits high bioavailability in living organisms. It also has significant mobility in natural environments [152]. Cr(VI) has been listed as a priority pollutant by several countries, and the World Health Organization recommends that the concentration of Cr in drinking water not exceed 0.05 mg/L [152]. Therefore, it is essential to minimize the formation of Cr(VI) through appropriate alloy composition and process control in the design of antifouling coatings containing Cr. Stabilizing Cr in its metallic Cr(0) or trivalent Cr(III) states can reduce the likelihood of oxidation to Cr(VI). Additionally, incorporating other corrosion-resistant metals, such as nickel or molybdenum, or applying stable passivation films can further inhibit the oxidation of Cr. Monitoring Cr(VI) release throughout the long-term use of such coatings is necessary to ensure their environmental safety. Future research should explore environmentally friendly alternatives to Cr in antifouling coatings or develop self-healing passivation coatings to maintain antifouling performance while minimizing environmental impact.

4. High entropy alloy coatings

High-entropy alloys [153–155], are a new class of alloys composed of multiple principal elements, typically five or more. With a rational combination and proportion of these elements, the high-entropy effect allows the alloy to form a simple phase structure, and the cocktail effect provides properties. Research has shown that in antibacterial tests using simulated seawater [121], the as-cast Al0.4CoCrCuFeNi high-entropy alloy releases many Cu ions, effectively inhibiting bacterial growth and biofilm formation. The antibacterial efficacy against *Pseudomonas aeruginosa* and *Bacillus vietnamensis*, two corrosive marine bacteria, was nearly 100 percent, demonstrating broad-spectrum antibacterial performance.

Figure 6 illustrates the Cu ion release concentrations and bacterial adhesion after 7 days of immersion in solutions containing these two bacteria for the high-entropy alloy and Cu-containing 304 stainless steel. In Figure 6a,b, the Cu ion release concentrations of

the alloys in *Pseudomonas aeruginosa* and *Bacillus vietnamensis* solutions were 5.7 ± 2.0 mg/L and 1.6 ± 0.2 mg/L for the high-entropy alloy, respectively, significantly higher than the 0.5 ± 0.2 mg/L and 0.01 ± 0.003 mg/L for the 304 Cu-containing stainless steel. Figure 6c,d depict the bacterial adhesion on the alloy surfaces after exposure to *Pseudomonas aeruginosa* and *Bacillus vietnamensis*. The high-entropy alloy exhibited substantially reduced bacterial adhesion, while the Cu-containing stainless steel still had considerable bacterial attachment, demonstrating the superior antibacterial properties of the high-entropy alloy.

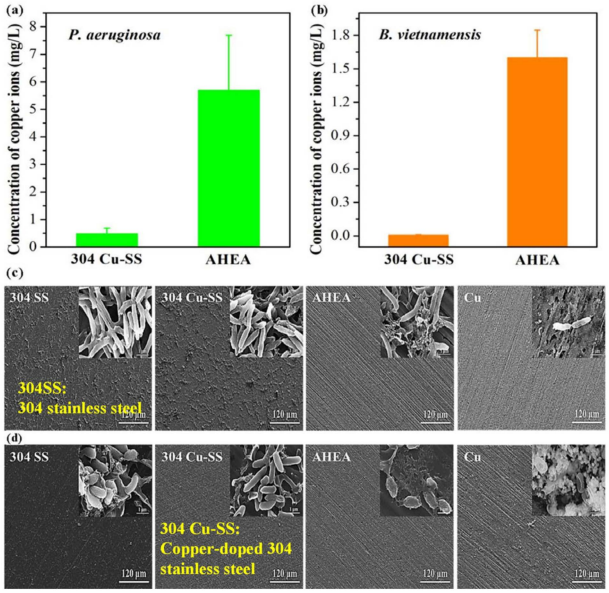

Figure 6. Cu ion release and bacterial adhesion: (**a**) ion concentration in *P. aeruginosa*, (**b**) ion concentration in *B. vietnamensis*, (**c**) adhesion of *P. aeruginosa* colonies, (**d**) adhesion of *B. vietnamensis* colonies [121].

To reduce Cu segregation in the alloy, research has employed SPS technology to fabricate AlCoCrFeNiCu0.5 high-entropy alloys [122]. By eliminating Cu segregation and achieving nanoscale Cu precipitation, the overall performance of the alloy was enhanced. The density of attached algae decreased to 135/mm^2, significantly lower than the 1973/mm^2 of the unmodified alloy. The wear rate of the alloy in seawater also reduced, with a wear rate of 6.5 × 10^{-6} mm^3/Nm, and the plastic strain increased by 1.65 times.

The study compares the effects of Cu by investigating CoCrFeNi and CoCrCuFeNi coatings applied to the surface of 249A steel via laser cladding [105]. In a marine environment, Cu in the CoCrCuFeNi coating gradually releases Cu ions, which gives the coating an antibacterial effect, reducing bacterial presence by 88%. Although the CoCrFeNi coating does not contain Cu, the alloy's nickel, cobalt, and chromium can also form metal ions that exhibit a certain level of toxicity to bacterial cells, thereby inhibiting bacterial growth. While the antibacterial performance of the CoCrFeNi coating is not as strong as the Cu-containing coating, the antibacterial properties of both high-entropy alloy coatings show significant improvement compared to the DMR 249A substrate. Regarding corrosion resistance, the corrosion rate of the CoCrFeNi coating is 0.0071 mm/year.

In comparison, that of the CoCrCuFeNi coating is 0.0086 mm/year, which is significantly lower than the corrosion rate of the DMR 249A substrate (0.0125 mm/year). This indicates that both high-entropy alloy coatings offer excellent corrosion resistance in a marine environment. As for wear resistance, the CoCrCuFeNi coating demonstrates superior performance with a wear rate of 4.63 × 10^{-10} mm^3/m, compared to 5.58 × 10^{-10} mm^3/m for the CoCrFeNi coating. This is attributed to the Cu in the CoCrCuFeNi, which oxidizes during friction to form CuO and Cu_2O, acting as a self-lubricating layer and thus enhancing the coating's wear resistance.

Table 2 summarizes the current major research findings and characteristics of copper-containing metal-based coatings. The antifouling mechanisms of these coatings are primarily based on the antibacterial properties of copper, as well as the regulation of copper ion release rates by other metal ions or structural components. The Cu-Fe alloy coating enhances copper release through the addition of iron and is characterized by its lower cost. The Cu-Ti alloy coating demonstrates durable antifouling performance at higher copper content, showcasing its effective antifouling capabilities. The Cu-Cr alloy coating improves performance by promoting the peeling of corrosion products, although attention must be paid to the environmental issues associated with hexavalent chromium. High-entropy alloy coatings exhibit significant antibacterial properties and superior corrosion resistance, while the characteristics of the high-entropy phase also provide the alloy with good mechanical properties. Future research could focus on selecting appropriate alloy compositions and coating designs based on different application needs to further enhance antifouling performance and environmental friendliness.

Table 2. Summary of research findings and characteristics of different copper-containing metal-based coatings.

Coating Type	Research Findings	Antifouling Mechanism	Characteristics
Cu-Fe coating	Ma et al. [42] found that a 12 wt% Fe coating has a Cu ion release rate of 40 μg/cm^2/day. The coating significantly inhibits microbial adhesion. Zhao et al. [39] reported that the adhesion strength of the 304L-Cu stainless steel coating is 69 MPa, with a low porosity of 0.34%.	Cu acts as the antibacterial component. Microchannels promote Cu ion release.	- Enhanced Cu release through Fe addition - Suitable for marine environments - Good self-repair capability - Lower coating cost
Cu-Ti coating	Tian et al. [79] found that when Cu content exceeds 19.2%, antifouling efficiency approaches 100%.	Cu acts as the antibacterial component. Microbattery structure uniformly releases Cu ions.	- Forms microbattery structure for long-lasting Cu release - Significantly improved antifouling performance with increased Cu content - Good wear resistance
Cu-Cr coating	Research [151] shows that the Cu ion release rate of a 5% Cr coating stabilizes at 40 μg/cm^2/day.	Cr promotes the peeling of corrosion products, enhancing Cu release.	- Improved antifouling performance with Cr addition - Environmental safety concerns (hexavalent chromium issue) - Suitable for long-term use
High-entropy alloy coating	Antibacterial efficiency is nearly 100%, and Cu ion release concentration is significantly higher than that of 304 stainless steel [121].	Inhibits bacterial growth by releasing Cu ions.	- Multi-element alloy provides comprehensive performance - Significant antibacterial effect, strong adaptability - Excellent corrosion and wear resistance

3.1.3. Cu-Doped Composite Coatings

1. Cu-Al_2O_3 composite coating

Al_2O_3 is a wear-resistant material and can be easily sourced. Additionally, as an inorganic coating, Al_2O_3 is not easily degraded by sunlight, thereby avoiding the secondary environmental pollution caused by the degradation of organic materials. By adding Cu as an antifouling element, the resulting coating offers both mechanical solid properties and antifouling capabilities. Guo et al. [61] produced a Cu/Al_2O_3 composite antifouling coating

on Q235 steel using low-pressure cold spraying technology. The Al_2O_3 layer is an insulation layer, protecting the substrate from galvanic corrosion, while the Cu layer collaborates with the Al_2O_3 layer to provide antifouling effects. Cold-sprayed coatings typically have lower porosity and a denser structure, which reduces the likelihood of microbial attachment, while flame-sprayed coatings are more prone to microvoids and defects, providing a more favorable environment for biofouling. Compared to flame-sprayed epoxy resin Al_2O_3 coatings, this cold-sprayed Cu/Al_2O_3 composite coating can inhibit 85.3% of the biofouling activities of barnacles, diatoms, and mussels.

Researchers have utilized plasma spraying to fabricate Cu-Al_2O_3 coatings with a micron-laminated structure, where the Al_2O_3 contents in the coatings are 32.1%, 51.6%, and 66.2%, respectively [81]. The micron-laminated structure produced by plasma spraying allows Cu to dissolve and be confined within microscopic channels. Adjusting the Al_2O_3 content allows the Cu ion release rate to be controlled. Figure 7 illustrates the layered structure of the coatings. In the pure Cu coating (Figure 7a), noticeable micropores and thin, band-like inclusions of Cu oxide are present. In the Cu-Al_2O_3 coatings (Figure 7b–d), the structure is more compact, with lower porosity. The dark gray stripes represent Al_2O_3, and the bright white stripes represent Cu splats. The Cu and Al_2O_3 layers are alternately and uniformly distributed, with thicknesses ranging from 1 to 5 microns. As the Al_2O_3 content increases, the continuity of the Al_2O_3 layers also improves. In the Cu-32.1% Al_2O_3 coating, the Al_2O_3 layers are discontinuous, while in the Cu-66.2% Al_2O_3 coating, the Al_2O_3 layers show a more continuous distribution.

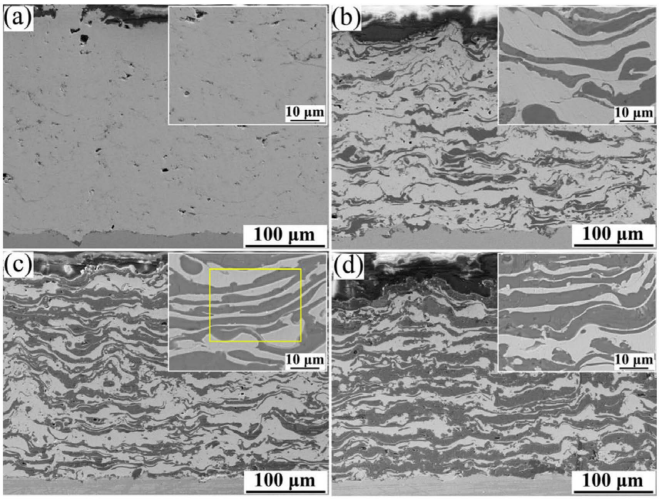

Figure 7. The cross-sections images of Cu-Al_2O_3 coatings with Al_2O_3 contents of (**a**) 0%, (**b**) 32.1%, (**c**) 51.6%, and (**d**) 66.2% [81].

Antifouling test results indicate that the Cu ion release rate of the Cu-Al_2O_3 coatings is five times lower than that of the pure Cu coating, which extends the antifouling performance of the coating and reduces Cu ion pollution in the environment. The release rate of the pure Cu coating is 52.5 μg/(cm^2·d), while the release rates for Cu-32.1% Al_2O_3, Cu-51.6% Al_2O_3, and Cu-66.2% Al_2O_3 coatings are 18.9 μg/(cm^2·d), 12.8 μg/(cm^2·d), and 10.1 μg/(cm^2·d), respectively. This demonstrates that introducing Al_2O_3 controls the slow release of Cu ions, thereby extending the antifouling performance. The wear tests found that the Al_2O_3 layers forming continuous trilayers enhanced the wear resistance, with the wear resistance of the Cu-66.2% Al_2O_3 coating being higher than the Cu-32.1% Al_2O_3 coating.

2. Cu/Cu_2O composite coating

In exploring the antifouling performance of different Cu-based composite coatings, researchers have also developed Cu/Cu_2O composite coatings to utilize the microcell effect between Cu and Cu_2O for Cu ion release. Ding et al. [62] prepared four different Cu/Cu_2O

composite coatings with varying Cu_2O levels (0%, 10%, 20%, and 30%) using cold spray technology. The antifouling mechanism of the coating primarily relies on the microcell effect between Cu_2O and Cu, where Cu_2O acts as the cathode and Cu as the anode. Additionally, Cu_2O can react with chloride ions in the seawater environment. The results show that as the Cu_2O increases, the microcell effect in the coating becomes more pronounced. The coating with 30% Cu_2O forms a more effective microcell structure, with a Cu ion release rate consistently above 50 $\mu g/cm^2/d$ in a stable state, effectively inhibiting the attachment of more than 90% of marine organisms, including microorganisms like diatoms. Although increasing the Cu_2O content can improve the antifouling effect, too much Cu_2O weakens the coating's bond strength, affecting its mechanical properties. Therefore, the optimal Cu_2O content for Cu/Cu_2O composite coatings is 30%.

3. Cu/GLC composite coating

Based on the low chemical reactivity and low friction coefficient characteristics of graphite-like carbon films, the researchers developed Cu/GLC composite antifouling coatings using magnetron sputtering. The graphene films refer to carbon films composed of a combination of sp^2- and sp^3-bonded carbon atoms, exhibiting properties similar to graphene, such as excellent chemical inertness and low friction. Zheng et al. [92] prepared Cu/GLC composite films with Cu contents ranging from 0 to 9.3at.% on 304 stainless steel using magnetron sputtering technology. The results showed that the tribological and antifouling performance of Cu/GLC films are improved due to the addition of Cu. The friction coefficient of pure GLC film is 0.125, while the average friction coefficients of Cu-doped GLC films are 0.096 (2.8 at.%), 0.090 (3.9 at.%), 0.060 (5.9 at.%), 0.080 (7.4 at.%), and 0.074 (9.3 at.%), indicating that Cu doping can improve their friction performance. The algae attachment rate of the pure GLC film was 4.62%, while the algae attachment rate decreased to 0.82% when the Cu content reached 5.9 at.%, and the surface of the 9.3 at.% Cu coating showed almost no algae attachment. Additionally, the addition of Cu significantly improved the coating's hydrophobicity, with the Cu/GLC coating achieving a maximum contact angle of 139° in artificial seawater and 98.5° in ethylene glycol solution when the Cu was 5.9%, reducing attachment of pollutants and marine organisms in water.

Figure 8 shows the HRTEM Images of Cu/GLC composite films. Figure 8a shows the typical amorphous structure of the GLC film. In the case of Cu/GLC films with Cu content of 5.9 at.%, Cu nanoparticles are embedded in the amorphous carbon matrix. In the case of Cu/GLC films with Cu content of 9.3 at.% (Figure 8c), the number and size of nanoparticles increased, and the diffraction spots corresponded to the (111), (200), (220), and (311) crystal planes of Cu. Additionally, the (200) crystal plane of Cu_2O is also visible in the diffraction pattern. Figure 8d–f show that at 9.3% Cu content, the Cu nanoparticles were uniformly distributed in the amorphous carbon matrix. In terms of corrosion resistance, these Cu-containing nanoparticles can form a dense physical barrier, preventing the penetration of corrosive media. In terms of antifouling, these Cu phases can release copper ions to provide antibacterial or anti-fouling effects, thereby inhibiting the attachment of microorganisms and contaminants.

4. Ti/(Cu, MoS_2) composite coatings

To further enhance the multifunctional properties of coatings, including self-lubrication, wear resistance, corrosion resistance, and antifouling performance, researchers have developed Ti/(Cu, MoS_2) composite coatings. Zhang et al. [93] designed Ti/(Cu, MoS_2) composite coatings with varying Cu content on 304 stainless steel to enhance its self-lubricating, wear-resistant, and corrosion-resistant properties. The design approach was as follows: Ti served as an adhesion layer; MoS_2 acted as a solid lubricant; and Cu was incorporated to enhance the coating's antifouling. The Ti/MoS_2 coating had a surface roughness of 2.99 nm and a hardness of approximately 16 GPa, but its antifouling performance was relatively poor. When the Cu content reached 5.3 at.%, the coating's self-lubricating and wear-resistant properties improved significantly, with the friction coefficient reduced to 0.036 and the wear rate to 5×10^{-8} $mm^3/N{\cdot}m$. The antifouling performance also im-

proved, with an algae attachment rate of 2.54%, indicating the proportion of the surface area covered by algae relative to the total surface area. A lower attachment rate reflects better antifouling performance, as it suggests reduced adhesion of algae and less biofouling on the coating surface.

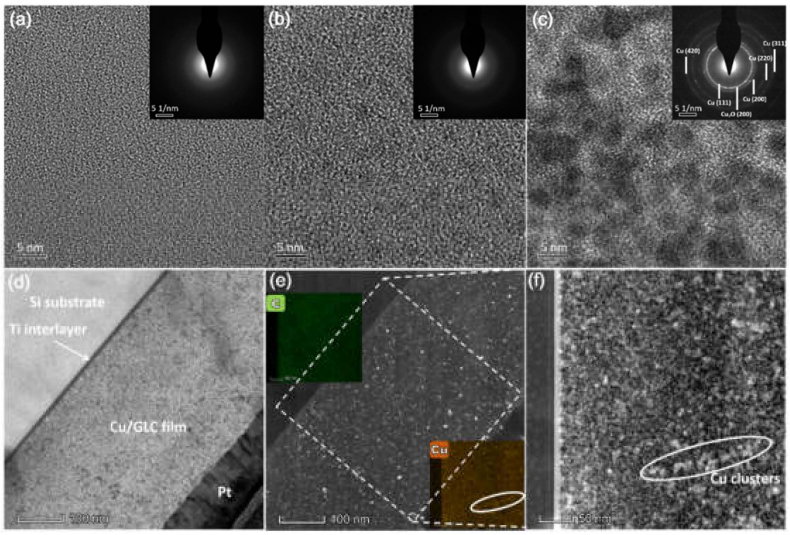

Figure 8. HRTEM of GLC (**a**), 5.9 at.% Cu (**b**), and 9.3 at.% Cu (**c**). TEM bright (**d**), dark (**e**), and HAADF-STEM (**f**) images for Cu (9.3 at.%)/GLC.3.1 zinc-doped polymer coatings [92].

As the Cu rose to 7.6 at.%, the coating achieved optimal self-lubricating, antifouling, and corrosion-resistant properties, with the algae attachment rate further reduced and with a contact angle of 91.5°, indicating good hydrophobicity. However, when the Cu was further increased to 9.0 at.%, the surface roughness increased to 10.80 nm. Although the hydrophobicity improved (with a contact angle of 101.6°), the self-lubricating and wear-resistant properties declined, with the friction coefficient rising to 0.064 and the wear rate increasing accordingly.

The corrosion resistance tests revealed that the corrosion performance of Ti/Cu-MoS_2-DLC coatings varied with the increase in Cu content. Polarization tests showed that the coating exhibited optimal corrosion resistance when the Cu content reached 7.6 at.% in the S3 sample, with the corrosion current density decreasing to 0.34×10^{-7} A/cm^2. EIS results further indicated that the S3 coating had the highest impedance modulus at low frequencies, demonstrating the formation of a dense and effective protective layer that significantly inhibited electrolyte penetration and corrosion. However, when the Cu content was too high in the S4 sample, the corrosion current density increased to 0.89×10^{-7} A/cm^2, indicating that excessive Cu reduced the protective effectiveness of the coating. These findings suggest that optimal corrosion resistance can be achieved by carefully controlling the Cu content, with the best balance obtained at 7.6 at.%.

Compared to Cu-doped polymer coatings, Cu-based metal coatings offer higher mechanical strength and wear resistance, achieving antifouling effects through the controlled release of Cu ions. However, in marine environments, Cu can form corrosion products that affect ion release rates and antifouling durability, necessitating alloy design and structural optimization to enhance coating performance. These coatings also face challenges in terms of cost and manufacturing technologies. For instance, Cu and its alloys are relatively expensive, and the technologies used (e.g., laser cladding, cold spraying, and plasma spraying) require complex, high-energy equipment, further raising production costs. Additionally, precise control over coating thickness, microstructure, and ion distribution during manufacturing directly impacts the coating's performance and cost efficiency.

Future research could optimize alloy compositions, explore synergies between Cu and other metals, and develop coatings with microchannels or multilayer structures to achieve

more durable and stable antifouling effects. Lowering production costs is also essential, as is improving process efficiency, reducing material waste, or using low-cost substitutes. Moreover, exploring environmentally friendly materials and processes, like developing non-toxic or low-toxicity alloy coatings and refining production methods to reduce energy consumption and environmental impact, is crucial. This approach enhances the sustainability of Cu-based metal coatings and ensures compliance with stricter environmental regulations, promoting sustainable development.

3.2. Ag-Doped Antifouling Coating

The use of Ag as an antimicrobial agent has a long history, dating back to ancient times [156]. As early as the pre-Christian era, ancient Egyptians used Ag vessels to store water, extending its shelf life. Similarly, the Greeks and Romans recognized the antibacterial properties of Ag, using Ag utensils to preserve drinks and food. Ag has been proven to possess broad-spectrum antibacterial activity and low environmental risk characteristics, showing potential as an antifouling material. However, due to the high cost of Ag, its application in marine antifouling remains primarily at the research stage. Current research mainly focuses on Ag-doped polymer coatings, Ag-doped inorganic coatings, and Ag-based composite coatings. This section will provide an overview of the characteristics of these Ag-based antifouling coatings and their recent developments.

3.2.1. Ag-Doped Polymer Coatings

In Ag-doped polymer coatings, the polymer usually acts as the matrix for structural support, while silver provides antifouling. Typically, the antifouling effect of silver is achieved through silver nanoparticles (AgNPs). AgNPs have been widely applied in water purification, biomedicine, and food preservation. Because of their wide range of uses, enduring antibacterial effects, and comparatively low environmental impact, AgNPs are considered an up-and-coming antifouling agent. Currently, research on Ag-doped polymers in the antifouling field is in its early stages, with existing studies primarily focusing on materials like natural urushiol and polydimethylsiloxane.

1. Polymeric urushiol/AgNP coatings

Urushiol is a naturally occurring organic compound extracted from lacquer trees. Its structure contains a catechol ring and a long alkyl side chain. Through polymerization, urushiol forms a crosslinked polymer known as polymeric urushiol (PUL), which possesses reducing, antioxidant, and antibacterial properties, functioning as a reductant, dispersant, and stabilizer [157,158]. Urushiol exhibits corrosion resistance and water resistance, making it suitable for use as a protective varnish. As a primer, appropriate doping with silver nanoparticles can enable antifouling and antibacterial performance by controlling the release of silver ions.

The study by Zheng et al. [159] utilized natural urushiol to reduce Ag nanoparticles within the coating in situ on 340 mm × 150 mm × 3 mm carbon steel plates, ensuring their uniform distribution within the polymer matrix. Experimental results showed that the coating without AgNPs demonstrated poor antibacterial and antifouling performance during testing. After 120 days of immersion in a marine environment, the surface of this coating exhibited significant attachment to aquatic organisms such as algae and barnacles. In contrast, the coating containing 0.05% AgNPs achieved antibacterial rates of 99.43% and 99.80% against *S. aureus* and *E. coli*. When the AgNP content increased to 0.1%, the antibacterial rate against *S. aureus* and *E. coli* reached 100%. However, it maintained a clean surface without noticeable microbial biofilm formation after 120 days of immersion, demonstrating long-term antifouling stability.

2. Polydimethylsiloxane/AgNP coatings

In superhydrophobic nanocomposite antifouling materials, the application of Ag as an antibacterial agent has shown recent advancements. Polydimethylsiloxane, due to its low surface energy, high flexibility, and excellent chemical stability, effectively repels water

and withstands mechanical abrasion when used in antifouling coatings. Ag nanoparticles also possess broad-spectrum antibacterial properties and low surface energy characteristics, further enhancing the coating's antifouling performance. Researchers prepared antifouling coatings using a solution casting method to disperse spherical Ag NPs uniformly at various concentrations within the PDMS matrix, with a thickness of 150 μm [160].

The study found that at Ag concentrations ranging from 0.01% to 0.1%, the nanoparticles were well-dispersed within the PDMS matrix, significantly improving the coating's hydrophobicity, with a contact angle reaching up to 148°. This created a smooth surface with low micro-roughness, effectively minimizing adhesion sites for microorganisms and achieving excellent antifouling performance. At a concentration of 0.5%, although the hydrophobicity slightly decreased compared to lower concentrations, the micro-roughness remained low, and the Ag NPs maintained effective antibacterial properties. However, when the concentration increased to 1% and 5%, the nanoparticles began to aggregate, increasing surface roughness and decreasing hydrophobicity. This study demonstrates that Ag NPs can form an effective antifouling coating with PDMS superhydrophobic materials. However, precise control of Ag concentration is required to achieve optimal antifouling performance.

3.2.2. Ag-Doped Inorganic Coatings

1. Graphene oxide-AgNP coatings

Graphene oxide is a two-dimensional carbon-based material with a unique nanostructure and abundant oxygen functional groups [161,162]. Its unique nanostructure is characterized by a two-dimensional planar form and layered features, which provide a large specific surface area at the nanoscale, increasing contact with other materials. The surface of graphene oxide contains numerous oxygen functional groups, such as carboxyl, hydroxyl, and ether groups, which offer multiple adhesion sites for the effective attachment of antimicrobial nanoparticles. These features provide numerous nucleation sites for the anchoring and growth of antimicrobial nanoparticles while also promoting uniform nanoparticle distribution and enhancing the stability of the coating.

Researchers have studied these properties based on graphene oxide/Ag nanoparticle antifouling coatings. Zhang et al. [163] investigated several composite materials with different Ag NP contents on polypropylene substrates, including GOA0.5, GOA1, and GOA2, representing mass ratios of GO to $AgNO_3$ of 0.5, 1, and 2, respectively. The coating preparation process is as follows: First, 125 mg of graphene oxide (GO) powder is dispersed in 437.5 mL of deionized water and treated with an ultrasonic probe for 10 min to ensure a uniform suspension. Next, a certain amount of 0.01 M silver nitrate ($AgNO_3$) solution is added to the suspension, followed by another 30 min of ultrasonic treatment. The mixture is then placed in an ice bath for 30 min to cool. Subsequently, sodium borohydride ($NaBH_4$) solution is added dropwise to the cooled mixture to reduce the silver ions on the surface of the GO, and the reaction is allowed to proceed at room temperature for 12 h. After the reaction is complete, the precipitate is collected by centrifugation and washed several times with deionized water and anhydrous ethanol to ensure the purity of the product. Finally, the washed composite is dried in a vacuum oven at 60 °C for 24 h. The dried GOA nanocomposite is then mixed with polyvinylidene fluoride (PVDF) at a mass ratio of 90:10, with NMP solvent added, and the mixture is processed by ball milling to form a uniform slurry. The prepared slurry is applied to a polypropylene (PP) substrate using the drop-coating method and dried at room temperature for 10 h, completing the coating preparation.

The results showed that the low Ag content GOA2 exhibited a uniform particle distribution and improved antifouling performance compared to GO without Ag nanoparticles. The medium Ag content GOA1 showed the best performance, with uniformly distributed Ag nanoparticles on GO, resulting in a homogeneous surface with the highest water contact angle (71°) and the lowest surface free energy (37.62 mN/m), achieving a biofilm inhibition rate of 83% against H. Pacifica and 56% against mixed algae. In contrast, the high Ag

content GOA0.5 showed reduced antifouling performance due to particle aggregation. This study also highlights that the distribution and state of Ag nanoparticles within the substrate must be considered when designing antifouling coatings.

2. Ag-doped CrN coatings

CrN, as a coating material, exhibits excellent mechanical properties such as high hardness and wear resistance. Cai et al. [91] fabricated CrN-Ag composite coatings on 316 L stainless steel substrates with dimensions 30 mm × 30 mm × 2 mm. Research on CrN-Ag composite coatings prepared by magnetron sputtering with different Ag contents has found that increasing Ag can enhance the antibacterial properties of the coating. Figure 9 shows the surface and cross-sectional morphology of CrN coatings and CrN-Ag composite coatings containing 4.9 at.%, 8.0 at.%, 13.1 at.%, and 18.3 at.% Ag, with coating thicknesses ranging from 2.1 to 3.5 μm as the Ag content increases. The alternating grey and bright areas represent CrN and Ag, respectively. The CrN coating exhibits large grain structures, indicating tightly packed particles that form a dense structure. When the Ag content is below 13.18 at.%, Ag is uniformly distributed in the CrN matrix; however, as the Ag content increases to 18.37 at.%, Ag particle aggregation occurs in the coating.

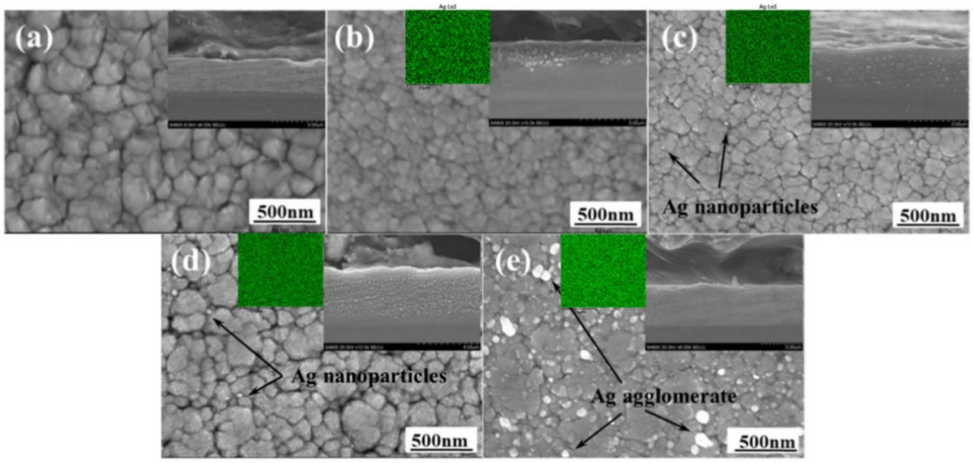

Figure 9. Top-view images and cross-sections of (**a**) CrN coating, (**b**) CrN-Ag coatings with 4.9 at.%, (**c**) 8.0 at.%, (**d**) 13.1 at.%, and (**e**) 18.3 at.% Ag [91].

Antibacterial tests show that the uniform distribution of Ag helps to improve the antibacterial and anti-algae effects of the coating; at 13.1 at.% Ag content, the coating reduces the adhesion of Chlorella by 45% and *Phaeodactylum tricornutum* by 64%, exhibiting optimal antifouling performance. However, when the Ag content increases to 18.3 at.%, the aggregation of Ag particles leads to an uneven coating structure, limiting the effective release of Ag ions and thus reducing the antibacterial effect.

Mechanical testing results show that the hardness of the CrN coating is approximately 16.3 GPa after incorporating 4.9 at.% Ag, and the hardness remains almost unchanged due to the limited effect of the small amount of Ag on the growth of CrN grains and microstructure. As the Ag content increases, the hardness decreases from 16.2 GPa to 8.0 GPa, primarily because Ag, a soft metal, softens the coating when embedded in the CrN matrix. On the other hand, with 4.9 at.% Ag, the solid solution strengthening effect increases the layer's elastic modulus, and adding Ag helps redistribute the load and enhance deformation resistance. However, as the Ag content further increases, the elastic modulus decreases. Low Ag content coatings, with finer grains and more grain boundaries, demonstrate better load-bearing capacity in nanoindentation tests. Overall, 13.1 at.% is the optimal Ag content for CrN-Ag coatings, as this level provides the best antifouling and antibacterial effects while maintaining good mechanical properties.

Corrosion resistance tests showed that the addition of silver made the corrosion potential of the coating more negative compared to pure CrN coatings, indicating an increased

thermodynamic tendency for corrosion. As the silver content increased from 4.9 at.% to 13.1 at.%, the corrosion potential decreased from −0.194 V to −0.241 V, and the corrosion current density significantly increased from 0.237 μA/cm^2 to 0.688 μA/cm^2, demonstrating a faster corrosion rate and reduced corrosion resistance. EIS tests further confirmed that the low-frequency impedance modulus decreased progressively with increasing silver content, indicating that corrosive media more easily penetrated the coating. However, when the silver content reached 18.3 at.%, silver aggregation caused the corrosion potential to rise to −0.211 V, and the corrosion current density decreased to 0.481 μA/cm^2, showing some improvement in corrosion resistance, though still inferior to coatings with lower silver content. These results indicate that while the addition of silver enhances electrical conductivity and antifouling properties, its content must be carefully controlled to prevent a significant reduction in corrosion resistance.

3. Ag-Al_2O_3 coatings

In the field of marine environment monitoring equipment protection, to address the issue of biofouling on optical windows, researchers have developed a composite coating based on a metal substrate combined with Ag antibacterial components, aimed at meeting the requirements for simple structure, long-lasting antifouling, and sufficient mechanical strength. Chen et al. [164] combined 3D printing technology to design a stainless steel mesh coated with an Ag film for marine observation window applications. To enhance the corrosion resistance of the 316SS mesh, an Al_2O_3 layer was first deposited as the base layer, followed by an Ag film coating on top.

Antifouling experiments demonstrated that after 30 days, the biofouling attachment rate on Ag-coated meshes was reduced by over 90% compared to untreated optical windows and uncoated meshes. A comparison of the 30#, 200#, and 800# mesh sizes of the 316SS substrates showed that the finer 800# mesh exhibited the best antifouling performance. This is attributed to its mesh structure, which enhances adhesion and effectively filters seawater pollutants, thereby reducing biofouling. Figure 10 shows the antifouling device, where the 800# mesh coated with Al_2O_3-Ag maintained a clean surface and exhibited the most effective antifouling performance. Corrosion resistance tests indicated that by adjusting the thickness and combination ratio of the coating layers, Al_2O_3 increased the impedance modulus of the coating to 7.26 kΩ·cm^2 in a simulated marine environment, significantly enhancing the coating's corrosion resistance. Compared to the single-layer Ag coating, the Al_2O_3/Ag double-layer coating demonstrated superior durability and stability in marine environments.

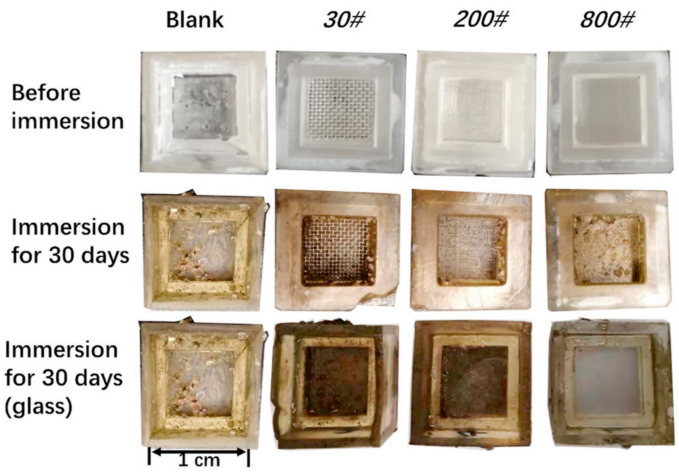

Figure 10. Comparison of optical windows with uncoated glass and those covered with Al_2O_3/Ag-coated 316SS meshes of varying sizes [164].

4. Cu-Ag co-doped antifouling coating

Cu and Ag ions both exhibit good antibacterial and antifouling properties. Combining Cu and Ag in a co-doped form theoretically can utilize their synergistic effects to enhance antifouling efficiency. Guo et al. [165] designed a Z-scheme structured CuOx/Ag/TiO_2 heterojunction coating on 304 stainless steel, where Ag was loaded onto TiO_2 using a wet chemical reduction method, followed by loading CuOx onto Ag/TiO_2 through a deposition–precipitation method to prepare the CuOx/Ag/TiO_2 composite. The study showed that combining CuOx and Ag could optimize the material's light absorption and photocatalytic efficiency. CuOx, being a narrow-band-gap metal oxide, enhanced the visible light absorption of TiO_2 and established a p-n heterojunction, facilitating the separation of photogenerated electron–hole pairs and minimizing their recombination. Furthermore, the localized surface plasmon resonance (LSPR) effect of Ag broadened the light absorption spectrum of TiO_2. It acted as an electron bridge, promoting the transfer of photogenerated electrons and improving photogenerated charges' separation and migration efficiency.

Under illumination, the photogenerated electrons of the CuOx/Ag/TiO_2 composite coating could be transferred to the metal surface, achieving cathodic protection. Experimental results showed that, under light irradiation, the open circuit potential of the CuOx/Ag/TiO_2 coating shifted negatively by approximately 240 mV, and the photocurrent density reached 16.6 $\mu A/cm^2$, indicating an improvement in photocatalytic corrosion resistance compared to the control material P25. The Cu^+ and Cu^{2+} in CuOx and Ag exhibited excellent antibacterial properties, effectively inhibiting microbial growth. The study results indicate that combining photocatalytic protection with chemical antibacterial action can achieve efficient corrosion resistance and antifouling, demonstrating the feasibility of application in marine environments.

Ag-doped antifouling coatings have broad potential applications, but there are certain limitations. Although Ag possesses excellent broad-spectrum antibacterial properties and low environmental risks, its high cost has restricted its application in marine antifouling, mainly to the research stage. Current studies on Ag-doped polymer and inorganic coatings suggest that the even dispersion of Ag nanoparticles and the regulation of ion release rates are key to maintaining long-term antifouling performance. However, ensuring antibacterial performance while reducing costs and preventing the aggregation of Ag particles within the coating remains a vital focus for future research.

Future studies could explore incorporating other low-cost metals or non-metallic elements and optimize the structural design of coatings to enhance cost-effectiveness and performance stability further. Additionally, developing more efficient dispersion technologies for Ag nanoparticles and new coating preparation methods may help reduce costs while maintaining antifouling efficacy, facilitating the practical application of Ag-doped antifouling coatings in marine environments.

Table 3 summarizes the research findings and characteristics of Ag-doped antifouling coatings. Each type of coating exhibits unique advantages in antifouling performance. For instance, polymeric urushiol combined with silver nanoparticles demonstrates excellent antibacterial properties and good corrosion resistance; polydimethylsiloxane coatings effectively reduce microbial adhesion due to their low surface energy; graphene oxide-based coatings leverage their unique nanostructure to ensure uniform distribution of silver nanoparticles, enhancing the stability and antifouling efficacy of the coating; and CrN-Ag coatings balance mechanical strength with antifouling performance. Future research could focus on selecting suitable alloy compositions and coating designs tailored to specific application needs.

Table 3. Summary of research findings and characteristics of Ag-doped antifouling coating.

Coating Type	Research Findings	Antifouling Mechanism	Characteristics
Polymeric urushiol/AgNP	Zheng et al. [159] found that 0.05% AgNPs achieved antibacterial rates of 99.43% and 99.80%.	Inhibits microbial growth through the release of silver ions and silver nanoparticles.	Naturally derived, excellent corrosion and antifouling properties.
Polydimethylsiloxane/AgNP	Research showed [160] that Ag concentrations from 0.01% to 0.1% significantly improved coating hydrophobicity.	Enhances surface hydrophobicity, minimizing adhesion sites for microorganisms.	Low surface energy, high flexibility, excellent chemical stability.
Graphene oxide-AgNP	Zhang et al. [163] found that medium Ag content coatings exhibited the best antifouling performance.	Uniform distribution of silver nanoparticles enhances antibacterial effects and inhibits biofilm formation.	Unique nanostructure provides good particle dispersion and stability.
CrN-Ag coatings	Cai et al. [91] found that 13.18 at.% Ag provided the optimal antifouling performance, reducing attachment rates.	Uniform distribution of silver particles improves antibacterial and anti-algal effects, reducing biofouling.	Excellent mechanical properties, high hardness, good antibacterial effects.
Ag-Al_2O_3 coatings	Chen et al. [164] showed that Ag-coated meshes reduced biofouling attachment by over 90%.	Releases silver ions effectively inhibiting microbial growth and preventing biofouling.	Combination with Al_2O_3 enhances corrosion resistance and mechanical strength.
Cu-Ag co-doped antifouling coating	Guo et al. [165] found that combining Cu and Ag optimized the material's light absorption and photocatalytic efficiency.	Photocatalytic generation of reactive oxygen species inhibits microbial growth while achieving cathodic protection.	Combines photocatalytic protection with chemical antibacterial action for effective antifouling and corrosion resistance.

4. Conclusions and Prospectives

This review systematically summarizes the leading preparation technologies of high-surface-strength antifouling coatings, including cold spray, plasma spray, magnetron sputtering, and laser cladding. It analyzes critical components, characteristics, and typical application cases of various coatings, such as Cu-doped polymer, Cu-doped metal, and Ag-doped antifouling coatings. These high-surface-strength antifouling coatings, especially metal-based coatings, show advantages in wear resistance, corrosion resistance, and service life. Different combinations of coatings and preparation techniques can provide targeted antifouling solutions for marine engineering equipment. In addition to antifouling performance, these coatings achieve overall performance by adjusting their composition and microstructure.

Although progress has been made in antifouling coating technology, practical applications still have many challenges and limitations. For example, many existing coatings may experience performance degradation due to biofouling and corrosion in extreme marine environments. How to develop coatings with longer service life and better antifouling and anticorrosion performance is an essential research focus in the future. In addition, traditional antifouling coating materials, such as Cu and Ag, while performing well in antibacterial and antifouling aspects, pose potential environmental risks that require stricter regulation and improvement to reduce negative impacts on marine ecosystems.

Future research directions can further expand in the following aspects:

Development of multifunctional antifouling coatings: Current antifouling coatings mainly focus on inhibiting microbial adhesion. Comprehensive coatings with antifouling, anticorrosion, wear resistance, and other multifunctional properties can be developed through material modification and functional composites. For example, introducing nanomaterials and smart polymers can provide self-healing properties to the coating, enhancing its durability and antifouling capacity.

Research on environmentally friendly antifouling coatings: Against the backdrop of increasing attention to environmental protection and sustainable development, researching and developing environmentally friendly antifouling coatings is becoming increasingly important. In the future, the composition of coating materials can be adjusted to reduce or replace toxic heavy metal elements, and antifouling coatings based on natural extracts and green materials can be developed to minimize potential harm to marine ecosystems.

Optimization of coating microstructure: The coating microstructure significantly impacts their antifouling performance, especially in controlling the microstructure at the nanoscale. Future research can optimize microstructure design by using nanoparticles and nanofibers to form an effective physical barrier, thereby improving coatings' antifouling and anticorrosion effects. Multilayer structure design can also achieve synergy among different functional materials, enhancing protective effects.

Improvement of coating preparation processes: The preparation process primarily affects the performance and application of coatings. In the future, preparation technologies such as cold spray, plasma spray, and laser cladding can be further optimized to improve their applicability to complex structures and large surfaces. Furthermore, novel preparation technologies such as micro-arc oxidation, high-energy laser cladding, and plasma-enhanced chemical vapor deposition also warrant in-depth research to improve coating quality, uniformity, and adhesion.

Research on antifouling performance in extreme environments: With the increasing development of deep-sea resources and polar exploration activities, the demand for antifouling coatings in extreme environments is gradually rising. Future research can optimize material composition and microstructure design to develop coatings capable of withstanding high pressure, low temperatures, and severe corrosion in deep-sea environments, meeting the needs of deep-sea mining equipment, polar research vessels, and other facilities.

Data-driven coating design: Leveraging advanced computational materials science and machine learning tools can accelerate the development of new antifouling coatings. Through extensive data analysis and simulation modeling, high-performance coating formulations can be screened more quickly, reducing the time and cost of experiments while helping to understand the complex relationships between different material components and antifouling performance.

Author Contributions: Conceptualization, X.S. and Y.L.; methodology, X.S.; validation, Y.L.; formal analysis, Y.L.; investigation, X.S.; resources, H.L.; data curation, X.S.; writing—original draft preparation, X.S.; writing—review and editing, X.S.; visualization, H.L.; supervision, H.L.; project administration, H.L.; funding acquisition, H.L. All authors have read and agreed to the published version of the manuscript.

Funding: The 2024 Anhui Provincial University Scientific Research Project (Natural Science Category, Key Project, No. 2024AH052003) and the 2024 Provincial Department of Education Science and Engineering Teachers' Internship Program in Enterprises (No. 2024jsqygz76).

Conflicts of Interest: The authors declare no conflicts of interest.

References

1. Dobson, T.; Yunnie, A.; Kaloudis, D.; Larossa, N.; Coules, H. Biofouling and corrosion rate of welded Nickel Aluminium Bronze in natural and simulated seawater. *Biofouling* **2024**, *40*, 193–208. [CrossRef] [PubMed]
2. Romeu, M.J.; Mergulhao, F. Development of Antifouling Strategies for Marine Applications. *Microorganisms* **2023**, *11*, 1568. [CrossRef] [PubMed]
3. Weber, F.; Esmaeili, N. Marine biofouling and the role of biocidal coatings in balancing environmental impacts. *Biofouling* **2023**, *39*, 661–681. [CrossRef] [PubMed]
4. Maduka, M.; Schoefs, F.; Thiagarajan, K.; Bates, A. Hydrodynamic effects of biofouling-induced surface roughness-Review and research gaps for shallow water offshore wind energy structures. *Ocean Eng.* **2023**, *272*, 113798. [CrossRef]
5. Soleimani, S.; Jannesari, A.; Etezad, S.M. Prevention of marine biofouling in the aquaculture industry by a coating based on polydimethylsiloxane-chitosan and sodium polyacrylate. *Int. J. Biol. Macromol.* **2023**, *245*, 125508. [CrossRef]

6. Yue, D.; Jiang, X.; Yu, H.; Sun, D. In-situ fabricated hierarchical nanostructure on titanium alloy as highly stable and durable super-lubricated surface for anti-biofouling in marine engineering. *Chem. Eng. J.* **2023**, *463*, 142389. [CrossRef]
7. Zou, Y.; Zhou, X.; Chen, L.; Xi, X. Impacts of different characteristics of marine biofouling on ship resistance. *Ocean Eng.* **2023**, *278*, 114415. [CrossRef]
8. Ghattavi, S.; Homaei, A. Synthesis and characterization of ZnO-SiO_2 hybrid nanoparticles as an effective inhibitor for marine biofilm and biofouling. *J. Mol. Liq.* **2024**, *396*, 123974. [CrossRef]
9. Kim, D.H.; Alayande, A.B.; Lee, J.M.; Jang, J.H.; Jo, S.M.; Jae, M.R.; Yang, E.; Chae, K.J. Emerging marine environmental pollution and ecosystem disturbance in ship hull cleaning for biofouling removal. *Sci. Total Environ.* **2024**, *906*, 167459. [CrossRef]
10. Ali, A.; Culliton, D.; Fahad, S.; Ali, Z.; Kang, E.-T.; Xu, L. Nature-inspired anti-fouling strategies for combating marine biofouling. *Prog. Org. Coat.* **2024**, *189*, 108349. [CrossRef]
11. Zheng, N.; Jia, B.; Liu, J.; Wang, X.; Zhang, D.; Zhang, H.; Wang, G. Multi-strategy combined bionic coating for long-term robust protection against marine biofouling. *J. Mater. Sci. Technol.* **2025**, *210*, 265–277. [CrossRef]
12. Kumar, A.; Mishra, V.; Negi, S.; Kar, S. A systematic review on polymer-based superhydrophobic coating for preventing biofouling menace. *J. Coat. Technol. Res.* **2023**, *20*, 1499–1512. [CrossRef]
13. Carrier, A.J.; Carve, M.; Shimeta, J.; Walker, T.R.; Zhang, X.; Oakes, K.D.; Jha, K.C.; Charlton, T.; Stenzel, M.H. Transitioning towards environmentally benign marine antifouling coatings. *Front. Mar. Sci.* **2023**, *10*, 1175270. [CrossRef]
14. Guo, H.; Yang, J.; Zhao, W.; Xu, T.; Lin, C.; Zhang, J.; Zhang, L. Direct formation of amphiphilic crosslinked networks based on PVP as a marine anti-biofouling coating. *Chem. Eng. J.* **2019**, *374*, 1353–1363. [CrossRef]
15. Saffarimiandoab, F.; Gul, B.Y.; Erkoc-Ilter, S.; Guclu, S.; Unal, S.; Tunaboylu, B.; Menceloglu, Y.Z.; Koyuncu, I. Evaluation of biofouling behavior of zwitterionic silane coated reverse osmosis membranes fouled by marine bacteria. *Prog. Org. Coat.* **2019**, *134*, 303–311. [CrossRef]
16. Harilal, M.; Anandkumar, B.; Lahiri, B.B.; George, R.P.; Philip, J.; Albert, S.K. Enhanced biodeterioration and biofouling resistance of nanoparticles and inhibitor admixed fly ash based concrete in marine environments. *Int. Biodeterior. Biodegrad.* **2020**, *155*, 105088. [CrossRef]
17. Xie, C.; Li, C.; Xie, Y.; Cao, Z.; Li, S.; Zhao, J.; Wang, M. ZnO/Acrylic Polyurethane Nanocomposite Superhydrophobic Coating on Aluminum Substrate Obtained via Spraying and Co-Curing for the Control of Marine Biofouling. *Surf. Interfaces* **2021**, *22*, 100833. [CrossRef]
18. Pedersen, M.L.; Weinell, C.E.; Ulusoy, B.; Dam-Johansen, K. Marine biofouling resistance rating using image analysis. *J. Coat. Technol. Res.* **2022**, *19*, 1127–1138. [CrossRef]
19. Aldred, N.; Anthony, C.S. The adhesive strategies of cyprids and development of barnacle-resistant marine coatings. *Biofouling* **2008**, *24*, 351–363. [CrossRef]
20. Pourhashem, S.; Seif, A.; Saba, F.; Nezhad, E.G.; Ji, X.; Zhou, Z.; Zhai, X.; Mirzaee, M.; Duan, J.; Rashidi, A.; et al. Antifouling nanocomposite polymer coatings for marine applications: A review on experiments, mechanisms, and theoretical studies. *J. Mater. Sci. Technol.* **2022**, *118*, 73–113. [CrossRef]
21. Liu, M.Y.; Li, S.N.; Wang, H.; Jiang, R.J.; Zhou, X. Research progress of environmentally friendly marine antifouling coatings. *Polym. Chem.* **2021**, *12*, 3702–3720. [CrossRef]
22. Liu, Z.H.; Zheng, X.Y.; Zhang, H.W.; Li, W.Y.; Jiang, R.J.; Zhou, X. Review on formation of biofouling in the marine environment and functionalization of new marine antifouling coatings. *J. Mater. Sci.* **2022**, *57*, 18221–18242. [CrossRef]
23. Chen, S.K.; Zhu, J.F.; Wang, B.C.; Liu, H.A.; He, B. Experimental Study on Hypochlorous Acid Blocking the Marine Diatom Adhesion. *Int. J. Electrochem. Sci.* **2012**, *7*, 5331–5338. [CrossRef]
24. Yi, J.; Ahn, Y.; Hong, M.; Kim, G.H.; Shabnam, N.; Jeon, B.; Sang, B.I.; Kim, H. Comparison between OCl^--Injection and In Situ Electrochlorination in the Formation of Chlorate and Perchlorate in Seawater. *Appl. Sci.* **2019**, *9*, 229. [CrossRef]
25. Shi, Z.Q.; Wang, T.; Zhao, J.; Qiu, R.; Duan, D.X.; Lin, C.G.; Wang, P. Pt nanostructure from electrodeposition: Electrocatalyst to generate chlorine for marine biofouling inhibition. *Colloids Surf. A-Physicochem. Eng. Asp.* **2017**, *520*, 522–531. [CrossRef]
26. Liu, Z.Z.; Zhang, Y.C.; Wang, T.Y.; Du, W.B.; Jin, H.C. ZnS:Cu/PDMS Composite Coating for Combating Marine Biofouling. *Coatings* **2023**, *13*, 2083. [CrossRef]
27. Lin, X.B.; Xie, Q.Y.; Ma, C.F.; Zhang, G.Z. Self-healing, highly elastic and amphiphilic silicone-based polyurethane for antifouling coatings. *J. Mater. Chem. B* **2021**, *9*, 1384–1394. [CrossRef]
28. Sun, J.W.; Liu, C.; Duan, J.Z.; Liu, J.; Dong, X.C.; Zhang, Y.M.; Wang, N.; Wang, J.; Hou, B.R. Facile fabrication of self-healing silicone-based poly(urea-thiourea)/tannic acid composite for anti-biofouling. *J. Mater. Sci. Technol.* **2022**, *124*, 1–13. [CrossRef]
29. Wei, C.Y.; Zhang, Y.; Tang, Z.; Zhang, C.A.; Wu, J.H.; Wu, B. Surface Reconstruction of Silicone-Based Amphiphilic Polymers for Mitigating Marine Biofouling. *Polymers* **2024**, *16*, 1570. [CrossRef]
30. Hu, P.; Xie, Q.Y.; Ma, C.F.; Zhang, G.Z. Silicone-Based Fouling-Release Coatings for Marine Antifouling. *Langmuir* **2020**, *36*, 2170–2183. [CrossRef]
31. Zhang, C.; Zhao, Z.R.; Lin, X.H.; Wang, S.B.; Wang, J.R.; Li, Y.C.; Li, Y.Q.; Zhang, Y.B.; Zhao, H.W. Molybdenum-14Rhenium alloy-The most promising candidate for high-temperature semiconductor substrate materials. *J. Alloys Compd.* **2024**, *991*, 174391. [CrossRef]
32. Yang, S.H.; Ringsberg, J.W.; Johnson, E.; Hu, Z.Q. Biofouling on mooring lines and power cables used in wave energy converter systems-Analysis of fatigue life and energy performance. *Appl. Ocean Res.* **2017**, *65*, 166–177. [CrossRef]

33. Gormley, K.; McLellan, F.; McCabe, C.; Hinton, C.; Ferris, J.; Kline, D.I.; Scott, B.E. Automated Image Analysis of Offshore Infrastructure Marine Biofouling. *J. Mar. Sci. Eng.* **2018**, *6*, 2. [CrossRef]
34. Piola, R.; Ang, A.S.; Leigh, M.; Wade, S.A. A comparison of the antifouling performance of air plasma spray (APS) ceramic and high velocity oxygen fuel (HVOF) coatings for use in marine hydraulic applications. *Biofouling* **2018**, *34*, 479–491. [CrossRef]
35. Yi, P.; Jia, H.Y.; Yang, X.S.; Fan, Y.; Xu, S.S.; Li, J.; Lv, M.L.; Chang, Y.J. Anti-biofouling properties of TiO_2 coating with coupled effect of photocatalysis and microstructure. *Colloids Surf. A-Physicochem. Eng. Asp.* **2023**, *656*, 130357. [CrossRef]
36. Sanz, D.S.; García, S.; Trueba, L.; Trueba, A. Bioactive Ceramic Coating Solution for Offshore Floating Wind Farms. *Transnav-Int. J. Mar. Navig. Saf. Sea Transp.* **2021**, *15*, 407–412. [CrossRef]
37. Wu, Y.D.; Li, Y.L.; Liu, X.L.; Wang, Q.J.; Chen, X.M.; Hui, X.D. High strength NiMnFeCrAlCu multi-principal-element alloys with marine application perspective. *Scr. Mater.* **2021**, *202*, 113992. [CrossRef]
38. Li, Y.X.; Yang, L.L.; Liao, Y.J.; Zhao, R.Z.; Ji, L.Z.; Su, R.; Xu, D.K.; Wang, F.H. Photothermal Heating-Assisted Superior Antibacterial and Antibiofilm Activity of High-Entropy-Alloy Nanoparticles. *Adv. Funct. Mater.* **2023**, *33*, 2302712. [CrossRef]
39. Zhao, J.; Lian, T.; Sun, Z.; Zhao, H.; Yang, C.; Fan, X.; Li, S.; Mao, J.; Deng, C.; Yang, K. Controllable release of Cu ions contributes to the enhanced environmentally-friendly performance of antifouling Cu-bearing stainless steel coating prepared using high-velocity air fuel. *Surf. Coat. Technol.* **2024**, *481*, 130629. [CrossRef]
40. Lian, T.Y.; Zhao, J.L.; Yang, C.G.; Yang, K. Environment-friendly antifouling coating of Cu-bearing stainless steel prepared by pre-alloyed powder. *Mater. Lett.* **2023**, *344*, 134439. [CrossRef]
41. Erinosho, M.F.; Akinlabi, E.T.; Pityana, S.; Owolabi, G. Laser Surface Modification of Ti6Al4V-Cu for Improved Microhardness and Wear Resistance Properties. *Mater. Res.-Ibero-Am. J. Mater.* **2017**, *20*, 1143–1152. [CrossRef]
42. Ma, H.R.; Liu, Z.D.; Li, J.X.; Liu, Q.B.; Zhang, J.; Wei, T.J. Optimization design of environmental-friendly Cu-Fe laser cladding coating for self-grown microchannel in a marine corrosive environment. *J. Alloys Compd.* **2023**, *940*, 168820. [CrossRef]
43. Vishwakarma, V.; Josephine, J.; George, R.P.; Krishnan, R.; Dash, S.; Kamruddin, M.; Kalavathi, S.; Manoharan, N.; Tyagi, A.K.; Dayal, R.K. Antibacterial copper-nickel bilayers and multilayer coatings by pulsed laser deposition on titanium. *Biofouling* **2009**, *25*, 705–710. [CrossRef] [PubMed]
44. Zhu, Y.B.; Dong, M.P.; Zhao, X.R.; Li, J.L.; Chang, K.K.; Wang, L.P. Self-healing of TiSiN/Ag coatings induced by Ag. *J. Am. Ceram. Soc.* **2019**, *102*, 7521–7532. [CrossRef]
45. Pounraj, S.; Somu, P.; Paul, S. Chitosan and graphene oxide hybrid nanocomposite film doped with silver nanoparticles efficiently prevents biofouling. *Appl. Surf. Sci.* **2018**, *452*, 487–497. [CrossRef]
46. Ashraf, P.M.; Shibli, S.M.A. Development of CeO_2- and TiO_2-incorporated aluminium metal-composite matrix with high resistance to corrosion and biofouling. *J. Solid State Electrochem.* **2008**, *12*, 315–322. [CrossRef]
47. Soethe, V.L.; Delatorre, R.G.; Ramos, E.M.; Parucker, M.L. TiO_2 thin Films for Biofouling Applications. *Mater. Res.-Ibero-Am. J. Mater.* **2017**, *20*, 426–431. [CrossRef]
48. Dayı, S.C.; Kılıçay, K. Repairing Al7075 surface using cold spray technology with different metal/ceramic powders. *Surf. Coat. Technol.* **2024**, *489*, 131124. [CrossRef]
49. Maharjan, N.; Ramesh, T.; Pham Duy, Q.; Zhai, W.; Ang, A.; Zhou, W. Post-processing of cold sprayed Ti6Al4V coating by laser shock peening. *J. Mater. Process. Technol.* **2024**, *330*, 118461. [CrossRef]
50. Judas, J.; Zapletal, J.; Adam, O.; Řehořek, L.; Jan, V. Microstructural stability and precipitate evolution of thermally treated 7075 aluminum alloy fabricated by cold spray. *Mater. Charact.* **2024**, *216*, 114259. [CrossRef]
51. Eyvazi, Z.; Abdollah-Zadeh, A.; Seraj, R.-A.; Azarniya, A. Effect of SiC content on the microstructure and wear behavior of cold-sprayed Al-SiC coatings deposited on AZ31 alloy substrate. *Surf. Coat. Technol.* **2024**, *489*, 131170. [CrossRef]
52. Li, W.; Xue, N.; Shao, L.; Wu, Y.; Qiu, T.; Zhu, L. Effects of spraying parameters and heat treatment temperature on microstructure and properties of single-pass and single-layer cold-sprayed Cu coatings on Al alloy substrate. *Surf. Coat. Technol.* **2024**, *490*, 131184. [CrossRef]
53. Behera, A.K.; Mantry, S.; Roy, S.; Pati, S. Improving bond strength and deposition efficiency of ceramic coatings via low pressure cold spraying: A study on hydroxyapatite coatings with Cu-Zn blends. *Surf. Coat. Technol.* **2024**, *494*, 131430. [CrossRef]
54. Tirukandyur, S.; Kandadai, V.A.; Ellingsen, M.; Petersen, J.B.; Jasthi, B.K. Effect of post-deposition heat treatment on microstructure and mechanical properties of NASA HR-1 cold spray coatings. *Surf. Coat. Technol.* **2024**, *482*, 130704. [CrossRef]
55. Li, N.; Wang, Q.; Niu, W.; Ge, S.; Han, P.; Guo, N. Recover the tensile strength of hard aluminum alloy through laser assisted cold spray. *Surf. Coat. Technol.* **2024**, *486*, 130966. [CrossRef]
56. Zhong, Y.; Liu, Z.; Zhang, Y.; Cha, L.; Ramachandran, C.S.; Wangm, Q. Microstructural and interfacial characteristics of supersonic reclaimed 2024Al-T3 substrate using cold sprayed 2024Al deposit. *Mater. Charact.* **2024**, *215*, 114158. [CrossRef]
57. Han, P.; Wang, Q.; Niu, W.; Ge, S.; Wan, M.; Li, N.; Qian, R. Bonding mechanism and fracture behavior of cold-sprayed Fe-based amorphous alloy on 6061 Al alloy. *Surf. Coat. Technol.* **2024**, *491*, 131194. [CrossRef]
58. Kılıçay, K. A practical approach to fabrication of nano-Al_2O_3 reinforced MMC coatings by cold spray: Characterization of nanomechanical and tribological performance. *Mater. Today Commun.* **2024**, *39*, 109257. [CrossRef]
59. Lett, S.; Cormier, J.; Quet, A.; Villechaise, P.; Meillot, E.; Hémery, S. Microstructure optimization of cold sprayed Ti-6Al-4V using post-process heat treatment for improved mechanical properties. *Addit. Manuf.* **2024**, *86*, 104168. [CrossRef]
60. Lupoi, R.; Stenson, C.; McDonnell, K.A.; Dowling, D.P.; Ahearne, E. Antifouling coatings made with Cold Spray onto polymers: Process characterization. *CIRP Ann.* **2016**, *65*, 545–548. [CrossRef]

61. Huang, G.; Xing, L.; Li, X.; Wang, H. Antifouling Behavior of a Low-Pressure Cold-Sprayed Cu/Al_2O_3 Composite Coating. *Int. J. Electrochem. Sci.* **2016**, *11*, 8738–8748. [CrossRef]
62. Ding, R.; Li, X.; Wang, J.; Li, W.; Wang, X.; Gui, T. Antifouling Properties and Release of Dissolved Copper of Cold Spray Cu/Cu_2O Coatings for Ships and Steel Structures in Marine Environment. *J. Mater. Eng. Perform.* **2018**, *27*, 5947–5963. [CrossRef]
63. Rui, D.; Haibin, Y.; Xiangbo, L. Electrochemical Corrosion and Mathematical Model of Cold Spray Copper Composite Coating—Part II: Limiting Current Region. *Int. J. Electrochem. Sci.* **2017**, *12*, 1232–1246. [CrossRef]
64. Rui, D.; Xiangbo, L.; Jia, W.; Likun, X. Electrochemical Corrosion and Mathematical Model of Cold Spray Cu-Cu_2O Coating in NaCl Solution—Part I: Tafel Polarization Region Model. *Int. J. Electrochem. Sci.* **2013**, *8*, 5902–5924. [CrossRef]
65. Stenson, C.; Mcdonnell, K.A.; Yin, S.; Aldwell, B.; Meyer, M.; Dowling, D.P.; Lupoi, R.J.; Taylor, F. Cold spray deposition to prevent fouling of polymer surfaces. *Surf. Eng.* **2018**, *34*, 193–204. [CrossRef]
66. Wang, Q.; Chai, H.; Zhang, X.; Song, Y.; Xi, Y.; Bai, S. Effect of powders recycling on microstructure evolution and wear mechanism of plasma sprayed Ni625-WC composite coating. *Surf. Coat. Technol.* **2024**, *494*, 131459. [CrossRef]
67. Yang, X.; Liu, Y.; Zhong, Y.; Chen, H. Anti/de-icing superhydrophobic coating with durability and self-healing by infiltrating photothermal self-stratifying organic layers into plasma-sprayed porous Al_2O_3–13%TiO_2 underlayer. *Surf. Interfaces* **2024**, *54*, 105305. [CrossRef]
68. Wu, L.; Zhang, K.; Yu, R.; Wang, G.; Zhou, Z.; Zhang, X. Discrepancy evaluation in mechanics and corrosion resistance of reactive plasma sprayed TiN coatings fabricated under different heat treatment. *Constr. Build. Mater.* **2024**, *446*, 138087. [CrossRef]
69. Nair, A.M.; Kumar, R.; Maurya, S.S.; Gaur, A.; Keshri, A.K.; Sharma, S. Plasma sprayed Titanium- Nanodiamond composite coatings with enhanced mechanical properties. *Mater. Today Commun.* **2024**, *41*, 110238. [CrossRef]
70. Zhao, K.; Huang, W.; Deng, P.; Zhong, R.; Hu, Y.; Li, J.; Mao, W. Mechanical properties, thermal shock resistance and stress evolution of plasma-sprayed 56wt% $Y2O_3$-stabilized ZrO_2 thick thermal barrier coatings. *Surf. Coat. Technol.* **2024**, *494*, 131352. [CrossRef]
71. Zhang, M.; Song, C.; Liu, M.; Yang, Y.; Du, K.; Liu, T.; Zhao, A.; Wen, K.; Deng, C.; Liao, H.; et al. Study on the performance of GDC electrolytes fabricated by atmospheric plasma spraying and vacuum plasma spraying. *Ceram. Int.* **2024**, *50*, 44391–44400. [CrossRef]
72. Wang, C.; Zhang, C.; Liu, M.; Huang, Y.; Wang, H.; Ma, G.; Zhou, X.; Jin, G. The effect of laser textured resin surface on the adhesion of supersonic plasma sprayed Al_2O_3/PF composite coating. *Surf. Coat. Technol.* **2024**, *487*, 130990. [CrossRef]
73. Hu, X.; Chen, Y.; Guo, H.; Xu, H. Corrosion behaviors and failure mechanism of plasma sprayed $Yb_2Si_2O_7$/Si environmental barrier coatings exposed to CMAS+ $NaVO_3$. *J. Eur. Ceram. Soc.* **2025**, *45*, 117005. [CrossRef]
74. Su, H.; Hu, H.; Chen, S.; Zhang, G.; Zhang, C. Tribological properties of atmospheric plasma sprayed Cr_3C_2–NiCr/20% nickel-coated graphite self-lubricating coatings. *Ceram. Int.* **2024**, *50*, 38040–38050. [CrossRef]
75. Chen, Z.Y.; Zhang, X.; Liang, Y.N.; Babar, Z.U.D.; Gao, J.; Li, W.M.; Zhang, S.L.; Li, C.J.; Li, C.X. Breakthrough in atmospheric plasma spraying of high-density composite electrolytes: Deposition behavior and performance of plasma-sprayed GDC-LSGM on porous metal-supported solid oxide fuel cells. *Int. J. Hydrog. Energy* **2024**, *72*, 614–625. [CrossRef]
76. Wang, X.Y.; Hu, Y.; Yang, Y.; Wang, Y.W.; Li, W.; Shao, Y.X.; Sun, W.W.; Zhao, H.J.; Ma, Y. Microstructure evolution and hardening mechanism of plasma-sprayed TiB2 nanocomposite coating. *J. Alloys Compd.* **2024**, *1007*, 176389. [CrossRef]
77. Wang, K.; Xu, K.W.; Tian, J.J.; Li, Z.Z.; Shao, G.S. Tailoring the Micro-galvanic Dissolution Behavior and Antifouling Performance Through Laminated-Structured Cu-X Composite Coating. *J. Therm. Spray Technol.* **2021**, *30*, 1566–1581. [CrossRef]
78. Tian, J.; Xu, K.; Hu, J.; Zhang, S.; Cao, G.; Shao, G. Durable self-polishing antifouling Cu-Ti coating by a micron-scale Cu/Ti laminated microstructure design. *J. Mater. Sci. Technol.* **2021**, *79*, 62–74. [CrossRef]
79. Tian, J.; Wang, K.; Xu, K.W.; Luo, X.T.; Shao, G.S.; Li, C.J. Effect of coating composition on the micro-galvanic dissolution behavior and antifouling performance of plasma-sprayed laminated-structured Cu-Ti composite coating. *Surf. Coat. Technol.* **2021**, *410*, 126963. [CrossRef]
80. Bi, S.Q.; Xu, K.W.; Shao, G.S.; Yang, K.; Tian, J.J. Mechanically robust antifouling coating with dual-functional antifouling strategy by infiltrating PDMS into plasma-sprayed porous Al_2O_3-Cu coating. *J. Mater. Sci. Technol.* **2023**, *159*, 125–137. [CrossRef]
81. Xu, K.W.; Tian, J.J.; Xie, S.F.; Wu, P. Facile Fabrication of Micron-Laminated Cu-Al_2O_3 Coating with Long-Lasting Antifouling Performance and Excellent Wear Resistance. *J. Therm. Spray Technol.* **2023**, *32*, 2170–2186. [CrossRef]
82. Atta, S.; Narendra Kumar, U.; Kumar, K.; Yadav, D.P.; Dash, S. Recent Developments and Applications of TiN-Based Films Synthesized by Magnetron Sputtering. *J. Mater. Eng. Perform.* **2023**, *32*, 9979–10015. [CrossRef]
83. Vetter, J.; Shimizu, T.; Kurapov, D.; Sasaki, T.; Mueller, J.; Stangier, D.; Esselbach, M. Industrial application potential of high power impulse magnetron sputtering for wear and corrosion protection coatings. *J. Appl. Phys.* **2023**, *134*, 160701. [CrossRef]
84. Chun, S.Y. Microstructures and Mechanical Properties of HfN Coatings Deposited by DC, Mid-Frequency, and ICP Magnetron Sputtering. *Corros. Sci. Technol.* **2023**, *22*, 393–398.
85. Mehr, A.K.; Mehr, A.K. Magnetron sputtering issues concerning growth of magnetic films: A technical approach to background, solutions, and outlook. *Appl. Phys. A-Mater. Sci. Process.* **2023**, *129*, 662. [CrossRef]
86. Tang, K.; Li, X.; Wang, C.; Shen, Y.; Xu, Y.; Wen, M. The application of NiCrPt alloy targets for magnetron sputter deposition: Characterization of targets and deposited thin films. *Thin Solid Film.* **2024**, *805*, 140501. [CrossRef]
87. Klein, P.; Hnilica, J.; Sochora, V.; Souček, P.; Fekete, M.; Vašina, P. Enhancement of ionized metal flux fraction without compromising deposition rate in industrial magnetron sputtering. *Surf. Coat. Technol.* **2024**, *489*, 131142. [CrossRef]

88. Deambrosis, S.M.; Zin, V.; Montagner, F.; Mortalò, C.; Fabrizio, M.; Miorin, E. Effect of temperature and deposition technology on the microstructure, chemistry and tribo-mechanical characteristics of Ti-B based thin films by magnetron sputtering. *Surf. Coat. Technol.* **2021**, *405*, 126556. [CrossRef]
89. Huo, Y.; Tan, Y.; Zhao, K.; Lu, Z.; Zhong, L.; Tang, Y. Enhanced electromagnetic wave absorption properties of Ni magnetic coating-functionalized SiC/C nanofibers synthesized by electrospinning and magnetron sputtering technology. *Chem. Phys. Lett.* **2021**, *763*, 138230. [CrossRef]
90. Kiryukhantsev-Korneev, P.V.; Sytchenko, A.D.; Gorshkov, V.A.; Loginov, P.A.; Sheveyko, A.N.; Nozhkina, A.V.; Levashov, E.A. Complex study of protective Cr_3C_2–NiAl coatings deposited by vacuum electro-spark alloying, pulsed cathodic arc evaporation, magnetron sputtering, and hybrid technology. *Ceram. Int.* **2022**, *48*, 10921–10931. [CrossRef]
91. Cai, Q.; Li, S.; Pu, J.; Bai, X.; Wang, H.; Cai, Z.; Wang, X. Corrosion resistance and antifouling activities of silver-doped CrN coatings deposited by magnetron sputtering. *Surf. Coat. Technol.* **2018**, *354*, 194–202. [CrossRef]
92. Zhang, J.; Zhou, S.; Wang, Y.; Wang, Y.; Wang, C.; Lu, X.; Mao, C.; Chen, S.; Lu, X.; Wang, L. Enhancing anti-corrosion and antifouling properties of Cu/GLC composite film for marine application. *Surface Coat. Technol.* **2019**, *375*, 414–426. [CrossRef]
93. Zhang, J.; Wang, Y.; Zhou, S.; Wang, Y.; Wang, C.; Guo, W.; Lu, X.; Wang, L. Tailoring self-lubricating, wear-resistance, anticorrosion and antifouling properties of Ti/(Cu, MoS_2)-DLC coating in marine environment by controlling the content of Cu dopant. *Tribol. Int.* **2020**, *143*, 106029. [CrossRef]
94. Sun, Z.L.; Evdokimov, K.E.; Konishchev, M.E.; Kuzmin, O.S.; Pichugin, V.F. Effect of post annealing on properties of N-doped TiO_2 films deposited by reactive magnetron sputtering. In Proceedings of the 14th International Conference on Films and Coatings, St. Petersburg, Russia, 14–16 May 2019.
95. Wang, B.; Wei, S.C.; Guo, L.; Wang, Y.J.; Liang, Y.; Huang, W.; Lu, F.J.; Chen, X.H.; Pan, F.S.; Xu, B.S. Original Effect of sputtering power on microstructure and corrosion properties of TiO_2 films deposited by reactive magnetron sputtering. *J. Mater. Res. Technol.* **2022**, *19*, 2171–2178. [CrossRef]
96. Li, C.; Zhang, M.Y.; Sun, Y.C.; Han, X. Research on the Thermal Fatigue Mechanism of Laser Cladding IN625 Process on Ductile Iron. *Int. J. Met.* **2024**, *18*, 3129–3151. [CrossRef]
97. Wang, K.Y.; Yin, X.Q.; Li, C.X.; Du, K.P.; Halifu, M. Study on the thermal behavior and microstructure of Fe-based deposited layers prepared by laser cladding on Al substrate. *Opt. Laser Technol.* **2024**, *179*, 111365. [CrossRef]
98. Han, T.F.; Ding, Z.M.; Feng, W.X.; Yao, X.Y.; Chen, F.F.; Gao, Y.S. Effects of Process Parameters on Microstructure and Wear Resistance of Laser Cladding A-100 Ultra-High-Strength Steel Coatings. *Coatings* **2024**, *14*, 669. [CrossRef]
99. Gu, B.; Zhang, H.; Wang, Y.; Xu, G.; Wang, C.; Gao, L.; Chu, J.; Yang, Y. Microstructure and corrosion properties of CrMnFeCoNi high entropy alloy coating by temperature field-assisted laser cladding. *Surf. Coat. Technol.* **2024**, *494*, 131473. [CrossRef]
100. Ge, H.; Ding, S.; Zhang, P.; Fang, H.; Hu, Y.; Yao, J. Influence of overlapping process on the distribution of Cr element in laser cladding 316L powder on 45# steel substrate. *Surf. Coat. Technol.* **2024**, *493*, 131249.
101. Li, Y.; Yuan, X.; Chen, Y.; Yang, G.; Ou, W.; Li, T. Improved microstructure and wear resistance of $(CoCrNi)_{82}Al_9Ti_9$ cladding layers via extreme high-speed laser cladding. *Surf. Coat. Technol.* **2024**, *494*, 131298. [CrossRef]
102. Wang, Q.Y.; Ma, W.Q.; Ji, Y.H.; Chai, H.; Zhang, X.S.; Xi, Y.C.; Dong, L.J.; Bai, S.L. Study on corrosion mechanism of laser-clad Ni-W_xC coating by in-situ electrochemical method under high temperature and pressure environment. *Mater. Today Commun.* **2024**, *41*, 110699. [CrossRef]
103. Nie, B.; Xue, Y.; Luan, B. Investigation on the interface microstructure and phase composition of laser cladding pure copper coating. *Surf. Coat. Technol.* **2024**, *494*, 131408. [CrossRef]
104. Liu, X.; Meng, L.; Zeng, X.; Zhu, B.; Cao, J.; Wei, K.; Hu, Q. Study on the microstructure, mechanical properties and cavitation erosion resistance of 17-4PH alloy coatings fabricated by high power laser cladding. *Surf. Coat. Technol.* **2024**, *494*, 131451. [CrossRef]
105. Verma, A.; Chauhan, L.; Kumar, T.S.; Singh, P.K.; Dommeti, S.G.; Thangaraju, S. Laser Cladding of CoCrCuFeNi and CoCrFeNi High-Entropy Alloys on DMR 249A Steel: Corrosion, Wear and Antibacterial Behaviour. *JOM* **2023**, *75*, 2701–2713. [CrossRef]
106. Shen, Y.; Liu, Z.D.; Kong, Y.; Wang, X.Y.; Li, J.X.; Ning, H.Q.; Pan, C.Y. Effect of Cr content on micro-galvanic dissolution behavior and corrosion characteristics of Cu-Cr alloy laser cladding layer in a simulated seawater environment. *Appl. Surf. Sci.* **2024**, *647*, 158972. [CrossRef]
107. Wang, R.Y.; Zhou, T.; Liu, J.; Zhang, X.W.; Yang, J.F.; Hu, W.B.; Liu, L. Designing novel anti-biofouling coatings on titanium based on the ferroelectric-induced strategy. *Mater. Des.* **2021**, *203*, 109584. [CrossRef]
108. Chen, X.W.; Tang, S.; Zhang, D.F.; Yan, J.Z.; Xie, W.L.; Ran, Q.Z. Influence of graphene on corrosion properties of micro arc oxidation coatings on 7075 aluminum alloy. *Int. J. Appl. Ceram. Technol.* **2024**, *21*, 3516–3525. [CrossRef]
109. Chen, X.W.; Tang, S.; Xie, W.L.; Zhang, M.; Song, H.; Ran, Q.Z.; Zhang, D.F.; Zeng, D.Z. Friction and wear behavior of micro-arc oxidation-modified graphene/epoxy resin composite coating on TC4 titanium alloy. *Mater. Werkst.* **2024**, *55*, 1037–1044. [CrossRef]
110. Liu, J.C.; Yin, H.; Xu, Z.Y.; Shao, Y.W.; Wang, Y.Q. Improving the Corrosion Resistance of Micro-Arc Oxidization Film on AZ91D Mg Alloy through Silanization. *Metals* **2024**, *14*, 569. [CrossRef]
111. Guo, Y.; Wei, M.; Tang, Z.; Chen, C.; Li, X.; Lu, X.; Zuo, W. Investigation of MoO_x/Al_2O_3 micro-arc oxidation coatings on corrosion performance based on AlSi10Mg selective laser-melted. *J. Alloys Compd.* **2024**, *1002*, 175292. [CrossRef]
112. Deng, M.; Zhang, P.; Kang, Z.; Mao, Y.; Xiong, Q.; Zhang, W.; Cai, Z.; Gu, L. Comparative study on the fretting and sliding wear properties of micro-arc oxidation-treated aluminum alloy at different temperatures. *Tribol. Int.* **2024**, *198*, 109847. [CrossRef]

113. Zhu, H.; Wu, C.; Xue, L.; Yang, L.; Liu, Y.; Wang, D.; Liang, Y.; Peng, Z. Effect of laser cleaning on the growth and properties of micro-arc oxidation layers of AZ31 magnesium alloy. *Surf. Coat. Technol.* **2024**, *488*, 131051. [CrossRef]
114. Li, Q.; Shang, J. Self-lubricating properties of $Al_2O_3/MoS_2/CePO_4$ composite layers in-situ prepared by micro arc oxidation on 6082-T6 alloy. *Mater. Today Commun.* **2024**, *40*, 110137. [CrossRef]
115. Liu, Z.; Lu, H.; Zhao, Z.; Zhu, Z.; Li, S. Influence of ultrasonic power modulation on the optimisation of aluminium alloy micro-arc oxidation coating properties. *Appl. Surf. Sci.* **2025**, *679*, 161067. [CrossRef]
116. Zhang, X.; Peng, Z.; Lu, X.; Lv, Y.; Cai, G.; Yang, L.; Dong, Z. Microstructural evolution and biological performance of Cu-incorporated TiO_2 coating fabricated through one-step micro-arc oxidation. *Appl. Surf. Sci.* **2020**, *508*, 144766. [CrossRef]
117. Hu, P.F.; Zhu, L.Y.; Liu, J.J.; Lv, Y.; Cai, G.Y.; Zhang, X.X. Effect of Ultrasonic Vibration on Microstructure and Antifouling Capability of Cu-Modified TiO_2 Coating Produced by Micro-Arc Oxidation. *Coatings* **2024**, *14*, 376. [CrossRef]
118. Kruzel, R.; Dembiczak, T.; Wachowicz, J. Optimization of Spark Plasma Sintering Technology by Taguchi Method in the Production of a Wide Range of Materials: Review. *Materials* **2023**, *16*, 5539. [CrossRef]
119. Xu, L.; Huang, K.H.; Guo, W.M.; Liu, Y.; You, Y.; Huang, Z.J.; Lin, H.T. B_4C-(Hf,Zr,Ta,Nb,Ti)B_2 composites prepared by reactive and non-reactive spark plasma sintering. *Ceram. Int.* **2023**, *49*, 19556–19560. [CrossRef]
120. Li, Z.; Tang, X.Z.; Zhu, W.Y.; Thompson, B.C.; Huang, M.Y.; Yang, J.L.; Hu, X.; Khor, K.A. Single-Step Process toward Achieving Superhydrophobic Reduced Graphene Oxide. *ACS Appl. Mater. Interfaces* **2016**, *8*, 10985–10994. [CrossRef]
121. Zhou, E.Z.; Qiao, D.X.; Yang, Y.; Xu, D.K.; Lu, Y.P.; Wang, J.J.; Smith, J.A.; Li, H.B.; Zhao, H.L.; Liaw, P.K.; et al. A novel Cu-bearing high-entropy alloy with significant antibacterial behavior against corrosive marine biofilms. *J. Mater. Sci. Technol.* **2020**, *46*, 201–210. [CrossRef]
122. Yu, Y.; Xu, N.; Zhu, S.; Qiao, Z.; Zhang, J.; Yang, J.; Liu, W. A novel Cu-doped high entropy alloy with excellent comprehensive performances for marine application. *J. Mater. Sci. Technol.* **2021**, *69*, 48–59. [CrossRef]
123. Zhou, Y.; Huang, Z.; Kong, D.; Zhou, W.; Lei, Y.; Zhang, L.; Dong, C. Applying bipolar electrochemistry to assess the corrosion mechanism of HVOF WC-based coatings with varies binders in different environments. *Surf. Coat. Technol.* **2024**, *477*, 130252. [CrossRef]
124. Singh, S.P.; Verma, P.K.; Singh, S.; Kapoor, M.; Balu, R. Microstructural characterization and electrochemical behaviour of HVOF sprayed WC-Co-Cr coatings on 316L boiler steel stainless steel. *Results Surf. Interfaces* **2024**, *16*, 100248. [CrossRef]
125. Zhang, Q.; Shao, L.; Li, W.; Cui, S.; Shang, L.; Wang, C.; Song, Q.; Zhang, C. Comparative study of anti-corrosion properties in different CrN/WC-Co duplex coatings processed by PVD/HVOF. *Surf. Coat. Technol.* **2024**, *483*, 130799. [CrossRef]
126. Halder, S.; Vinay, G.; Anupam, A.; Ang, A.S.; Mahajan, D.K.; Singh, H. Effect of prolonged immersion on corrosion and cavitation resistance of HVOF-sprayed WC-NiCr and WC-Hastelloy cermet coatings. *Surf. Coat. Technol.* **2024**, *494*, 131384. [CrossRef]
127. Liu, L.; Shao, L.; Li, W.; Shang, L.; Zhu, B.; Wang, C.; Song, Q.; Zhang, C. Effect of different HVOF coatings on the tribological behavior of PVD/HVOF duplex coatings. *Tribol. Int.* **2024**, *198*, 109873. [CrossRef]
128. Daniel, J.; Dulišković, J.; Skála, O.; Liška, K.; Buršíková, V.; Fořt, T.; Houdková, Š. Influence of thickness and surface roughness on impact wear and impact lifetime of HVOF-sprayed coatings. *Surf. Coat. Technol.* **2024**, *488*, 131058. [CrossRef]
129. Yang, M.; Jin, Q.; Huang, T.; Kong, D.; Song, P. Effect of Cr_3C_2 distribution on the wear and corrosion properties of HVOF-sprayed WC–12Co/Cr_3C_2–25NiCr composite coatings. *Ceram. Int.* **2024**, *50*, 19720–19732. [CrossRef]
130. Litovchenko, N.V.; Potanin, A.Y.; Zamulaeva, E.I.; Sukhorukova, I.V.; Pogozhev Yu, S.; Gloushankova, N.A.; Ignatov, S.G.; Levashov, E.A.; Shtansky, D.V. Combustion synthesis of Ti-C-Co-$Ca_3(PO_4)_2$-Ag-Mg electrodes and their utilization for pulsed electrospark deposition of bioactive coatings having an antibacterial effect. *Surf. Coat. Technol.* **2017**, *309*, 75–85. [CrossRef]
131. Sheveyko, A.N.; Manakova, O.S.; Zamulaeva, E.I.; Kudryashov, A.E.; Potanin, A.Y.; Sukhorukova, I.V.; Zhitnyak, I.Y.; Gloushankova, N.A.; Levashov, E.A.; Shtansky, D.V. Structural transformations in TiC-CaO-$Ti_3PO_{(x)}$-(Ag_2Ca) electrodes and biocompatible TiCaPCO(N)-(Ag) coatings during pulsed electrospark deposition. *Surf. Coat. Technol.* **2016**, *302*, 327–335. [CrossRef]
132. Kudryashov, A.E.; Potanin, A.Y.; Lebedev, D.N.; Sukhorukova, I.V.; Shtansky, D.V.; Levashov, E.A. Structure and properties of Cr–Al–Si–B coatings produced by pulsed electrospark deposition on a nickel alloy. *Surf. Coat. Technol.* **2016**, *285*, 278–288. [CrossRef]
133. Zamulaeva, E.I.; Levashov, E.A.; Sviridova, T.A.; Shvyndina, N.V.; Petrzhik, M.I. Pulsed electrospark deposition of MAX phase Cr_2AlC based coatings on titanium alloy. *Surf. Coat. Technol.* **2013**, *235*, 454–460. [CrossRef]
134. Zamulaeva, E.I.; Zinovieva, M.V.; Kiryukhantsev-Korneev Ph, V.; Petrzhik, M.I.; Kaplanskii, Y.Y.; Klechkovskaya, V.V.; Sviridova, T.A.; Shvyndina, N.V.; Levashov, E.A. Protective coatings deposited onto LPBF-manufactured nickel superalloy by pulsed electrospark deposition using $MoSi_2$-MoB-HfB_2 and $MoSi_2$-MoB-ZrB_2 electrodes. *Surf. Coat. Technol.* **2021**, *427*, 127806. [CrossRef]
135. Zamulaeva, E.I.; Sheveyko, A.N.; Potanin, A.Y.; Zhitnyak, I.Y.; Gloushankova, N.A.; Sukhorukova, I.V.; Shvindina, N.V.; Ignatov, S.G.; Levashov, E.A.; Shtansky, D.V. Comparative investigation of antibacterial yet biocompatible Ag-doped multicomponent coatings obtained by pulsed electrospark deposition and its combination with ion implantation. *Ceram. Int.* **2018**, *44*, 3765–3774. [CrossRef]
136. Piola Richard, F.; Dafforn Katherine, A.; Johnston Emma, L. The influence of antifouling practices on marine invasions. *Biofouling* **2009**, *25*, 633–644. [CrossRef]

137. Hawkins, S.J.; Evans, A.J.; Mieszkowska, N.; Adams, L.C.; Bray, S.; Burrows, M.T.; Firth, L.B.; Genner, M.J.; Leung, K.M.Y.; Moore, P.J.; et al. Distinguishing globally-driven changes from regional- and local-scale impacts: The case for long-term and broad-scale studies of recovery from pollution. *Mar. Pollut. Bull.* **2017**, *124*, 573–586. [CrossRef]
138. Grimón, R.O.R.; Osorio, M.F.A.; de Freitas, D.M.; Castro, I.B. Tributyltin impacts in Galapagos Islands and Ecuadorian shore: Marine protected areas under threat. *Mar. Policy* **2016**, *69*, 24–31. [CrossRef]
139. Ookubo, N.; Nakamura, S.; Miyakusu, K. Antimicrobial activity and basic properties of antimicrobial stainless steel 'NSSAM Series'. *Nisshin Steel Tech. Rep.* **1998**, *77*, 69–81.
140. Wang, S.; Guo, X.; Yang, H.; Dai, J.; Zhu, R.; Gong, J.; Peng, L.; Ding, W. Electrodeposition mechanism and characterization of Ni–Cu alloy coatings from a eutectic-based ionic liquid. *Appl Surf Sci.* **2014**, *288*, 530–536. [CrossRef]
141. Hong, I.T.; Koo, C.H. Antibacterial properties, corrosion resistance and mechanical properties of Cu-modified SUS 304 stainless steel. *Mater. Sci. Eng. A* **2005**, *393*, 213–222. [CrossRef]
142. Zhang, X.Y.; Huang, X.B.; Jiang, L.; Ma, Y.; Fan, A.L.; Tang, B. Antibacterial Property of Cu Modified Stainless Steel by Plasma Surface Alloying. *J. Iron Steel Res. Int.* **2012**, *19*, 75–79. [CrossRef]
143. Nan, L.; Yang, K. Effect of Cu addition on antibacterial property of type 200 stainless steel. *Mater. Technol.* **2016**, *31*, 44–47. [CrossRef]
144. Wang, S.; Yang, K.; Shen, M.; Yang, C. Effect of Cu content on antibacterial activity of 17-4 PH stainless steel. *Mater. Technol.* **2015**, *30*, B115–B119.
145. Nan, L.; Yang, W.C.; Liu, Y.Q.; Xu, H.; Li, Y.; Lu, M.Q.; Yang, K. Antibacterial mechanism of copper-bearing antibacterial stainless steel against *E*. coli. *J. Mater. Sci. Technol.* **2008**, *24*, 197–201.
146. Bagley, F.; Atlar, M.; Charles, A.; Anderson, C. The use of copper-based antifoulings on aluminium ship hulls. *Ocean Eng.* **2015**, *109*, 595–602. [CrossRef]
147. Zhang, Y.; Fu, S.; Yang, L.; Qin, G.; Zhang, E. A nano-structured $TiO_2/CuO/Cu_2O$ coating on Ti-Cu alloy with dual function of antibacterial ability and osteogenic activity. *J. Mater. Sci. Technol.* **2022**, *97*, 201–212. [CrossRef]
148. Zhu, W.; Zhang, Z.; Gu, B.; Sun, J.; Zhu, L. Biological Activity and Antibacterial Property of Nano-structured TiO_2 Coating Incorporated with Cu Prepared by Micro-arc Oxidation. *J. Mater. Sci. Technol.* **2013**, *29*, 237–244. [CrossRef]
149. Miller, R.J.; Adeleye, A.S.; Page, H.M.; Kui, L.; Lenihan, H.S.; Keller, A.A. Nano and traditional copper and zinc antifouling coatings: Metal release and impact on marine sessile invertebrate communities. *J. Nanopart. Res.* **2020**, *22*, 129. [CrossRef]
150. Ding, T.; Xu, L.; Liu, X.; Ma, L.; Cui, Y.; Li, D.; Sun, X.; Gao, C. A Cu_2O-based marine antifouling coating with controlled release of copper ion mediated by amphiphilic PLMA-b-PDMAEMA copolymers. *Prog. Org. Coat.* **2022**, *170*, 107003. [CrossRef]
151. Shen, Y.; Liu, Z.; Kong, Y.; Li, B. A comparative study on the inhibition of microalgae attachment performance between Cu-based alloy laser cladding layer containing submicron Cr-rich precipitated phases and copper in simulated seawater. *J. Alloys Compd.* **2024**, *992*, 174642. [CrossRef]
152. Shi, X.C.; Wang, K.; Xue, M.; Mao, W.; Xu, K.; Tremblay, P.L.; Zhang, T. Ultrafast removal of toxic Cr(VI) by the marine bacterium Vibrio natriegens. *Chemosphere* **2024**, *350*, 141177. [CrossRef] [PubMed]
153. Gorban, V.F.; Andreev, A.A.; Stolbovy, V.A.; Firstov, S.A.; Karpets, M.V.; Danylenko, M.I. Properties of Metal, Nitride, Oxide, and Carbide Coatings Produced from High-Entropy Alloys. *Powder Metall. Met. Ceram.* **2023**, *62*, 469–480. [CrossRef]
154. Hsu, W.L.; Tsai, C.W.; Yeh, A.C.; Yeh, J.W. Clarifying the four core effects of high-entropy materials. *Nat. Rev. Chem.* **2024**, *8*, 471–485. [CrossRef]
155. Huang, S.S.; Zhang, J.; Fu, H.J.; Xiong, Y.X.; Ma, S.H.; Xiang, X.P.; Xu, B.; Lu, W.Y.; Zhang, Y.W.; Weber, W.J.; et al. Irradiation performance of high entropy ceramics: A comprehensive comparison with conventional ceramics and high entropy alloys. *Prog. Mater. Sci.* **2024**, *143*, 101250. [CrossRef]
156. Talapko, J.; Matijević, T.; Juzbašić, M.; Antolović-Požgain, A.; Škrlec, I. Antibacterial Activity of Silver and Its Application in Dentistry, Cardiology and Dermatology. *Microorganisms* **2020**, *8*, 1400. [CrossRef]
157. Chen, J.; Zhao, J.; Lin, F.; Zheng, X.; Jian, R.; Lin, Y.; Wei, F.; Lin, Q.; Bai, W.; Xu, Y. Polymerized tung oil toughened urushiol-based benzoxazine copper polymer coatings with excellent antifouling performances. *Prog. Org. Coat.* **2023**, *177*, 107411. [CrossRef]
158. Chen, J.; Jian, R.; Yang, K.; Bai, W.; Huang, C.; Lin, Y.; Zheng, B.; Wei, F.; Lin, Q.; Xu, Y. Urushiol-based benzoxazine copper polymer with low surface energy, strong substrate adhesion and antibacterial for marine antifouling application. *J. Clean. Prod.* **2021**, *318*, 128527. [CrossRef]
159. Zheng, L.; Lin, Y.C.; Wang, D.H.; Chen, J.P.; Yang, K.; Zheng, B.B.; Bai, W.B.; Jian, R.K.; Xu, Y.L. Facile one-pot synthesis of silver nanoparticles encapsulated in natural polymeric urushiol for marine antifouling. *RSC Adv.* **2020**, *10*, 13936–13943. [CrossRef]
160. Selim, M.S.; El-Safty, S.A.; El-Sockary, M.A.; Hashem, A.I.; Elenien, O.M.A.; El-Saeed, A.M.; Fatthallah, N.A. Modeling of spherical silver nanoparticles in silicone-based nanocomposites for marine antifouling. *RSC Adv.* **2015**, *5*, 63175–63185. [CrossRef]
161. Khan, M.; Tahir, M.N.; Adil, S.F.; Khan, H.U.; Siddiqui, M.R.H.; Al-warthan, A.A.; Tremel, W. Graphene based metal and metal oxide nanocomposites: Synthesis, properties and their applications. *J. Mater. Chem. A* **2015**, *3*, 18753–18808. [CrossRef]
162. Georgakilas, V.; Tiwari, J.N.; Kemp, K.C.; Perman, J.A.; Bourlinos, A.B.; Kim, K.S.; Zboril, R. Noncovalent Functionalization of Graphene and Graphene Oxide for Energy Materials, Biosensing, Catalytic, and Biomedical Applications. *Chem. Rev.* **2016**, *116*, 5464–5519. [CrossRef] [PubMed]
163. Zhang, X.X.; Mikkelsen, O. Graphene Oxide/Silver Nanocomposites as Antifouling Coating on Sensor Housing Materials. *J. Clust. Sci.* **2022**, *33*, 627–635. [CrossRef]

164. Chen, C.; Wang, Y.; Ge, F.F. Construction of corrosion resistant stainless steel mesh and the design for protecting optical window free from biofouling. *Ocean Eng*. **2022**, *264*, 112564. [CrossRef]
165. Guo, X.M.; Pan, G.T.; Fang, L.N.; Liu, Y.; Rui, Z.B. Z-Scheme CuO_x/Ag/TiO_2 Heterojunction as Promising Photoinduced Anticorrosion and Antifouling Integrated Coating in Seawater. *Molecules* **2023**, *28*, 456. [CrossRef]